1

2 **Title: The localization of PHRAGMOPLAST ORIENTING KINESIN1 at the division site depends
3 on two microtubule binding proteins TANGLED1 and AUXIN-INDUCED-IN-ROOT-CULTURES9
4 in Arabidopsis.**

5

6 **Running title:** Determinants of POK1 localization

7

8

9 Alison M. Mills[1], Victoria H. Morris[2,3], Carolyn G Rasmussen[1,2,*]

10

11 [1]Graduate Group in Biochemistry and Molecular Biology
12 [2]Department of Botany and Plant Sciences, Center for Plant Cell Biology, Institute of Integrative
13 Genome Biology, University of California, Riverside.
14 [3]Current address: Brandeis University, Waltham, MA

15

16

17 [*]Correspondence to Carolyn Rasmussen: carolyn.rasmussen@ucr.edu

18

19 ORCID CGR 0000-0002-4354-6295
20 ORCID AMM 0000-0002-7391-1409
21 ORCID VHM 0000-0003-4881-6343

22

23 **Keywords:** mitosis, cytokinesis, TANGLED1, AIR9, phragmoplast, POK1, division plane orientation,
24 Arabidopsis

25

26 **One sentence summary:** Specific amino acids within TAN1 are required for its correct localization
27 and function partially through interaction with POK1; both TAN1 and AIR9 mediate POK1 division
28 site localization.

29

30

31

32 **Abstract:**

33 Proper plant growth and development requires spatial coordination of cell divisions. Two unrelated

34 microtubule-binding proteins, TANGLED1 (TAN1) and AUXIN-INDUCED-IN-ROOT-CULTURES9

35 (AIR9), are together required for normal growth and division-plane orientation in Arabidopsis.

36 *tan1 air9* double mutants have synthetic growth and division-plane orientation defects while single

37 mutants lack obvious defects. Here we show that the division-site localized protein,

38 PHRAGMOPLAST-ORIENTING-KINESIN1 (POK1), was aberrantly lost from the division site during

39 metaphase and telophase in *tan1 air9* mutants. Since TAN1 and POK1 interact via the first 132

40 amino acids of TAN1 (TAN1$_{1-132}$), we assessed its localization and function in the *tan1 air9* double

41 mutant. TAN1$_{1-132}$ rescued *tan1 air9* mutant phenotypes and localized to the division site in

42 telophase. However, replacing six amino-acid residues within TAN1$_{1-132}$ that disrupts POK1-TAN1

43 interaction in the yeast-two-hybrid system caused loss of both rescue and division-site localization

44 of TAN1$_{1-132}$ in *tan1 air9* mutants. Full-length TAN1 with the same alanine substitutions had defects

45 in phragmoplast guidance and reduced TAN1 and POK1 localization at the division site but rescued

46 most *tan1 air9* mutant phenotypes. Together, these data suggest that TAN1 and AIR9 are required

47 for POK1 localization, and yet unknown proteins may stabilize TAN1-POK1 interactions.

48
49
50 **Introduction**
51 Division plane orientation is important for many aspects of plant, microbial, and animal
52 development, particularly growth and patterning. Division plane orientation is especially relevant
53 for plant cells which are encased in cell walls, and unable to migrate (Rasmussen and Bellinger,
54 2018; Livanos and Müller, 2019; Facette et al., 2018; Wu et al., 2018). Positioning and construction
55 of the new cell wall (cell plate) during cytokinesis involves two microtubule- and microfilament-
56 rich cytoskeletal structures, the preprophase band (PPB) and the phragmoplast respectively
57 (Smertenko et al., 2017). The PPB is a ring of microtubules, microfilaments, and proteins that forms
58 at the cell cortex just beneath the plasma membrane during G2: this region is defined as the cortical
59 division zone (Van Damme, 2009; Smertenko et al., 2017; Li et al., 2015). The cortical division zone
60 is characterized by active endocytosis mediated by TPLATE-clathrin coated vesicles that may
61 deplete actin and the actin-binding kinesin like-protein KCA1/KAC1 (Vanstraelen et al., 2004;
62 Suetsugu et al., 2010; Karahara et al., 2009; Kojo et al., 2013; Panteris, 2008; Hoshino et al., 2003).
63 After nuclear envelope breakdown, the PPB disassembles and the metaphase spindle, an
64 antiparallel microtubule array with its plus-ends directed toward the middle of the cell, forms (Dixit
65 and Cyr, 2002). After the chromosomes are separated, the phragmoplast is constructed from
66 spindle remnants to form another antiparallel array of microtubules (Lee and Liu, 2019). The
67 phragmoplast microtubules are tracks for the movement of vesicles containing cell wall materials
68 towards the forming cell plate (McMichael and Bednarek, 2013; Müller and Jürgens, 2016). The
69 phragmoplast expands by nucleation of new microtubules on pre-existing microtubules (Murata et
70 al., 2013; Smertenko et al., 2018) and is partially dependent on the mitotic microtubule binding
71 protein ENDOSPERM DEFECTIVE1 and the augmin complex to recruit gamma tubulin to
72 phragmoplast microtubules (Lee et al., 2017; Nakaoka et al., 2012). Finally, the phragmoplast
73 reaches the cell cortex and the cell plate and associated membranes fuse with the mother cell
74 membranes at the cell plate fusion site previously specified by the PPB (van Oostende-Triplet et al.,
75 2017).
76
77 TANGLED1 (TAN1, AT3G05330) was the first protein identified to localize to the plant division site
78 throughout mitosis and cytokinesis (Walker et al., 2007). In maize, the *tan1* mutant has defects in
79 division plane orientation caused by phragmoplast guidance defects (Cleary and Smith, 1998;
80 Martinez et al., 2017). TAN1 bundles and crosslinks microtubules in vitro (Martinez et al., 2020). In
81 vivo, TAN1 promotes microtubule pausing at the division site (Bellinger et al., 2021). TAN1,
82 together with other division site localized proteins, is critical for the organization of an array of cell
83 cortex localized microtubules that is independent from the phragmoplast. These cortical-telophase
84 microtubules accumulate at the cell cortex during telophase and are subsequently incorporated
85 into the phragmoplast to direct its movement towards the division site (Bellinger et al., 2021).
86 Other important division site localized proteins were identified through their interaction with
87 TAN1, such as the division site localized kinesin-12 proteins PHRAGMOPLAST ORIENTING
88 KINESIN1 (POK1) and POK2 (Müller et al., 2006; Lipka et al., 2014). Similar to other kinesin-12
89 proteins, PHRAGMOPLAST ASSOCIATED KINESIN RELATED PROTEIN (PAKRP1) and PAKRPL1
90 (Lee et al., 2007; Pan et al., 2004), POK2 localizes to the phragmoplast midline during telophase and

2

91 plays a unique role in phragmoplast expansion (Herrmann et al., 2018). Together, POK1 and POK2
92 are required to guide the phragmoplast to the division site (Herrmann et al., 2018; Müller et al.,
93 2006). *pok1 pok2 Arabidopsis thaliana* (Arabidopsis) double mutants have stunted growth and
94 misplaced cell walls as a result of phragmoplast guidance defects (Müller et al., 2006). The *pok1*
95 *pok2* double mutants also fail to maintain TAN1 at the division site after entry into metaphase
96 (Lipka et al., 2014). This suggests that TAN1 maintenance at the division site after metaphase is
97 dependent on POK1 and POK2.
98
99 In Arabidopsis, *tan1* mutants have very minor phenotypes (Walker et al., 2007). However,
100 combination of *tan1* with *auxin-induced-in-root-cultures9* (*air9),* a mutant with no obvious defects
101 (Buschmann et al., 2015), resulted in a synthetic phenotype consisting of reduced root growth,
102 increased root cell file rotation and phragmoplast guidance defects (Mir et al., 2018). TAN1 and
103 AIR9 are unrelated microtubule-binding proteins that both localize to the division site (Walker et
104 al., 2007; Buschmann et al., 2006). Both TAN1 and AIR9 colocalize with the PPB. TAN1 remains at
105 the division site throughout cell division, while AIR9 is lost from the division site upon PPB
106 disassembly and then reappears at the division site during cytokinesis when the phragmoplast
107 contacts the cortex. When full length *TAN1* fused to *YELLOW FLUORESCENT PROTEIN* (*TAN1-YFP*)
108 and driven either by the constitutive viral cauliflower mosaic *CaMV35S* promoter (*p35S:TAN1-YFP*)
109 or the native promoter with the fluorescent protein as either N- or C-terminal fusion (*pTAN1:TAN1-*
110 *YFP* or *pTAN1:CFP-TAN1*) was transformed into the *tan1 air9* double mutant, the phenotype was
111 rescued such that plants looked similar to and grew as well as wild-type plants (Mir et al., 2018;
112 Mills and Rasmussen, 2022).
113
114 TAN1 is an intrinsically disordered protein with no well-defined domains. It was divided into five
115 conserved regions based on alignments of amino acid similarity across plant species. Region I,
116 which covers the first ~130 amino acids of TAN1, is the most highly conserved, and mediates TAN1
117 localization to the division site during telophase. This ~130 amino acid region also mediates
118 interactions between TAN1 and POK1 in the yeast-two-hybrid system (Rasmussen et al., 2011).
119 When *TAN1* missing the first ~130 amino acids was transformed into the *tan1 air9* double mutant,
120 no rescue was observed (Mir et al., 2018). This suggests that the first ~130 amino acids of the TAN1
121 protein are critical for function in root growth and division plane positioning.
122
123 Here, we show that both AIR9 and TAN1 are required for POK1 to remain at the division site after
124 PPB disassembly. We identified TAN1-POK1 interaction motifs within the first 132 amino acids
125 using the yeast-two-hybrid system. Interestingly, the first 132 amino acids of TAN1 (TAN1$_{1-132}$) are
126 sufficient to rescue the *tan1 air9* double mutant, but not when a TAN1-POK1 interaction motif was
127 disrupted. We found that when full-length TAN1 with the same mutated motif was used, substantial
128 rescue was observed, except defects in phragmoplast guidance and loss of POK1 and TAN1 at the
129 division site during metaphase and telophase. Together, this suggests that interactions between
130 POK1 and AIR9, and TAN1 and POK1, as well as other yet unknown proteins, are important for
131 division plane orientation and plant growth.
132
133

Results:

Either TAN1 or AIR9 is sufficient to recruit and maintain POK1 at the division site

To understand how known division-site localized proteins interact at the division site, we examined POK1 fused to YELLOW FLUORESCENT PROTEIN (YFP-POK1 (Lipka et al., 2014)) localization in wild type, *tan1 air9* double mutants and single mutants expressing the microtubule marker *UBQ10:mScarlet-MAP4* (Pan et al., 2020). Our hypothesis was that POK1 localization would not be contingent on TAN1 or AIR9, and would therefore be unaltered in the *tan1 air9* double mutant. In contrast to our hypothesis, YFP-POK1 was lost from the division site during metaphase and telophase and also accumulated less frequently during preprophase and prophase. In wild-type cells, YFP-POK1 colocalized with PPBs in 71% of preprophase/prophase cells (n = 50/70 cells, 15 plants, Figure 1A) consistent with previous observations (Schaefer et al., 2017). In the *tan1 air9* double mutant, YFP-POK1 colocalized with 50% of PPBs during preprophase/prophase, which was not significantly different than wild-type (n = 27/54 cells, 15 plants, Figure 1D; Table 1; Fisher's exact test, P-Value = 0.0165, ns with Bonferroni correction). In wild-type cells, YFP-POK1 remained at the division site in all observed metaphase (n = 13/13 cells, Figure 1B) and telophase cells (n = 31/31 cells, Figure 1C), similar to previous studies (Lipka et al., 2014). In rare instances, YFP-POK1 also accumulated in the phragmoplast midline in wild-type cells (13%, n = 4/31, 11 plants, Table 1). In contrast, in *tan1 air9* mutants, YFP-POK1 was lost from the division site in metaphase (n = 0/21 cells, Figure 1E; Table 1) and telophase (n = 0/44, Figure 1F). Interestingly, in *tan1 air9* double mutants, although YFP-POK1 did not accumulate at the division site, it accumulated at the phragmoplast midline in 77% of cells (n = 34/44), significantly more frequent midline accumulation than the 13% observed in wild-type plants (n = 4/31 cells, Table 1; Fisher's exact test, P-value < 0.00001). Together, this shows that POK1 is not maintained at the division site after PPB disassembly and that instead it accumulates in the phragmoplast midline. We hypothesize that mislocalized phragmoplast midline accumulation of YFP-POK1 in *tan1 air9* mutants occurs because YFP-POK1 is not maintained at the division site.

Next, we examined YFP-POK1 localization in *tan1* and *air9* single mutants. YFP-POK1 localized to the division site during all mitotic stages, but aberrantly accumulated in the phragmoplast midline in *tan1* single mutants. Similar to wild-type plants, YFP-POK1 colocalized with PPBs during preprophase or prophase in *tan1* mutants (Figure 1G) and *air9* mutants (Figure 1H), and remained at the division site during metaphase and telophase (Figure 1G-L, Table 1). In *tan1* single mutants, YFP-POK1 localized both to the division site and the phragmoplast midline in 44% of telophase cells (Figure 1I, n = 12/27), which is significantly more midline accumulation compared to wild-type plants (13%, n = 4/31, 10 plants, Fisher's exact test, P-value = 0.0094) or *air9* single mutants (Figure 1L, 10%, n = 4/40). Aberrant phragmoplast midline accumulation of YFP-POK1 in the *tan1* single mutants suggested that POK1-TAN1 interaction might be required to maintain POK1 at the division site. This prompted us to examine their interaction more closely.

Amino acids 1-132 of TAN1 Rescue the *tan1 air9* Double Mutant

POK1 interacts with both full-length TAN1 and the first 132 amino acids of TAN1 using the yeast-two-hybrid system (Rasmussen et al., 2011). In addition, TAN1 missing the first 126 amino acids

3

177 failed to rescue the *tan1 air9* double mutant, suggesting that this part of the protein is critical for
178 TAN1 function (Mir et al., 2018). To test the function of this region of the protein in Arabidopsis, the
179 *TAN1* coding sequence for the first 132 amino acids was fused to YFP (TAN1$_{1-132}$-YFP) driven by the
180 cauliflower mosaic *p35S* promoter and was then transformed into the *tan1 air9* double mutant. We
181 used *p35S:TAN1-YFP* in the *tan1 air9* double mutant as our benchmark for rescue, as its ability to
182 rescue the *tan1 air9* double mutant was demonstrated previously (Mir et al., 2018). The progeny of
183 several independent *p35S:TAN1$_{1-132}$-YFP* lines rescued the *tan1 air9* double mutant, as described in
184 more detail below. Overall root patterning of *tan1 air9* double mutants expressing either
185 *p35S:TAN1$_{1-132}$-YFP* or full-length *p35S:TAN1-YFP* was restored, while untransformed *tan1 air9*
186 double mutant roots had misoriented divisions (Figure 2A, Supplementary Figure 1). Cell file
187 rotation, which skews left and has large variance in the *tan1 air9* double mutant (Figure 2B & 2C),
188 was significantly rescued in both *p35S:TAN1$_{1-132}$-YFP* and *p35S:TAN1-YFP tan1 air9* lines (n = 37 and
189 41 plants respectively), compared to the untransformed *tan1 air9* control (Levene's test used due
190 to non-normal distribution, P-value < 0.0001). Root length at 8 days after stratification was also
191 restored (Figure 2D). Interestingly, although TAN1$_{1-132}$-YFP rarely co-localizes with PPBs in wild-
192 type plants (Rasmussen et al., 2011) or in *tan1 air9* double mutants (10%, n = 9/89 cells, Figure
193 3A), PPB angles of *p35S:TAN1$_{1-132}$-YFP* and *p35S:TAN1-YFP tan1 air9* plants had significantly less
194 variance compared to the untransformed control (Figure 2E). Phragmoplast positioning defects of
195 the *tan1 air9* double mutant were also significantly rescued by *p35S:TAN1$_{1-132}$-YFP*. Altogether,
196 *p35S:TAN1$_{1-132}$-YFP* rescued the phenotypes of the double mutant similar to full-length *p35S:TAN1-*
197 *YFP.* This indicates that most functions that affect phenotypes assessed here are encoded by the
198 first section of the *TAN1* gene.
199
200
201 **Disrupting TAN1-POK1 interaction alters TAN1 and POK1 localization to the division site**
202 **and reduces *tan1 air9* rescue**
203 To further understand how TAN1 functions, we disrupted its ability to interact with the kinesin
204 POK1 using alanine scanning mutagenesis. Alanine scanning mutagenesis was used to replace six
205 amino acids with six alanines across the first ~120 amino acids of TAN1$_{1-132}$ (described in materials
206 and methods). After testing their interaction with POK1 using the yeast-two-hybrid system, we
207 identified seven constructs that lost interaction with POK1 (Supplementary Figure 2). Reasoning
208 that highly conserved amino acids would be more likely to play critical roles in TAN1-POK1
209 interaction, we selected TAN1$_{1-132}$ with alanine substitutions replacing the highly conserved amino
210 acids 28-33 (INKVDK) with six alanines (TAN1(28-33A)$_{1-132}$) for analysis in Arabidopsis. Our
211 hypothesis was that the mutated form of TAN1$_{1-132}$ (TAN1(28-33A)$_{1-132}$) would not rescue the *tan1*
212 *air9* mutant due to lack of POK1 and TAN1 interaction. *TAN1(28-33A)$_{1-132}$* was cloned into a plant
213 transformation vector to generate *p35S:TAN1(28-33A)$_{1-132}$-YFP* and transformed into the *tan1 air9*
214 double mutant. The *p35S:TAN1(28-33A)$_{1-132}$-YFP* construct partially rescued the *tan1 air9* double
215 mutant (Figure 4). *p35S:TAN1(28-33A)$_{1-132}$-YFP* in the *tan1 air9* double mutant did not rescue cell
216 file rotation defects (Figure 4B, D) or phragmoplast angle defects (Figure 4F). However, overall
217 plant growth (Figure 4C) and root length (Figure 4E) showed intermediate rescue compared to
218 unaltered *p35S:TAN1$_{1-132}$-YFP* in the *tan1 air9* double mutant. PPB angles in *tan1 air9* double
219 mutants expressing either *p35S:TAN1(28-33A)$_{1-132}$-YFP* or *p35S:TAN1$_{1-132}$-YFP* were similar,

220   suggesting that TAN1-POK1 interaction may not be required for PPB placement (Figure 4F). These
221   results suggest that the first 132 amino acids of TAN1 perform several vital functions, some of
222   which are contingent or partially contingent on a likely interaction with POK1 in Arabidopsis.
223

224   To understand how this mutation within TAN1$_{1-132}$ affected localization, we analyzed TAN1(28-
225   33A)$_{1-132}$-YFP in the *tan1 air9* double mutant. Localization of TAN1(28-33A)$_{1-132}$-YFP to the division
226   site in *tan1 air9* double mutants was significantly reduced compared to unaltered TAN1$_{1-132}$-YFP,
227   which localized to the division site during telophase 100% of the time (n = 58/58 cells, 29 plants,
228   Figures 3E, (Rasmussen et al., 2011)). TAN1(28-33A)$_{1-132}$-YFP showed no obvious division site
229   localization 68% of the time (n = 15/22 cells, Figure 3I) or faint division site accumulation in 32%
230   of telophase cells (n = 7/22 cells, Figure 3J). When the fluorescence intensity of TAN1(28-33A)$_{1-132}$-
231   YFP at the division site during telophase was compared to the cytosolic fluorescence intensity in the
232   same cell, the median ratio was ~1.1 indicating little preferential accumulation of TAN1(28-33A)$_{1-}$
233    $_{132}$-YFP at the division site (Figure 3K). In contrast, the median ratio of unaltered TAN1$_{1-132}$-YFP at
234   the division site was ~1.8 compared to cytosolic fluorescence, indicating its preferential
235   accumulation at the division site. This suggests that TAN1 requires the motif in amino acids 28-33
236   to localize properly to the division site during telophase. Our hypothesis is that this reduced
237   localization is due to disruptions in TAN1$_{1-132}$-POK1 interaction.
238

239   Next, we generated a construct that introduced alanines at amino acids 28-33 in full-length YFP-
240   TAN1 constructs (*p35S:YFP-TAN1(28-33A))* to assess whether *p35S:YFP-TAN1(28-33A)* would
241   rescue the *tan1 air9* double mutant. In contrast to the modest partial rescue provided by
242   *p35S:TAN1(28-33A)$_{1-132}$-YFP*, full-length *p35S:YFP-TAN1(28-33A)* significantly rescued the defects in
243   the *tan1 air9* double mutant, as described below. First, we assessed whether full-length TAN1(28-
244   33A) interacted with POK1 via the yeast-two-hybrid system, and it did not (Supplementary Figure
245   3). Next, we analyzed rescue in Arabidopsis expressing p*35S:YFP-TAN1(28-33A).* Most defects
246   except phragmoplast angle variance (Figure 5, Supplementary Figure 4) were fully rescued in the
247   *p35S:YFP-TAN1(28-33A) tan1 air9* lines, including cell file rotation (Figure 5C), root length (Figure
248   5D) and PPB angles (Figure 5E). Similar to TAN1-YFP, YFP-TAN1(28-33A) localized to the division
249   site in preprophase, prophase and telophase (Supplementary Figure 5).
250

251   To determine if full-length YFP-TAN1(28-33A) had reduced accumulation at the division site during
252   telophase similar to TAN1(28-33A)$_{1-132}$-YFP, fluorescence intensity levels were measured. During
253   prophase, YFP-TAN1(28-33A) fluorescence intensity at the division site compared to the cytosol
254   was comparable to TAN1-YFP fluorescence intensity ratios. In contrast, YFP-TAN1(28-33A)
255   fluorescence intensity ratios during telophase were reduced to ~1.6 compared with unaltered
256   TAN1-YFP (~2.1) indicating that YFP-TAN1(28-33A) accumulated less at the division site during
257   telophase (Supplementary Figure 5). Together, these data suggest that TAN1 is recruited to the
258   division site during prophase without interaction with POK1. Defects in phragmoplast positioning
259   may be due specifically to the disruption of TAN1-POK1 interaction, or due to the lower
260   accumulation of TAN1 at the division site that would normally be mediated by POK1 during
261   telophase.
262

263   To better understand how these alanine substitutions affect both POK1 and TAN1 localization we
264   examined *tan1 air9* double mutants expressing a microtubule marker (*UBQ10:mScarlet-MAP4* (Pan
265   et al., 2020)), *pTAN1:CFP-TAN1(28-33A)* and *pPOK1:YFP-POK1* (Lipka et al., 2014). Both CFP-
266   TAN1(28-33A) and YFP-POK1 had reduced accumulation at the division site in the *tan1 air9* double
267   mutant. CFP-TAN1(28-33A) and YFP-POK1 colocalized with the PPB in 41% of cells (n = 32/79)
268   which is significantly less frequent when compared to 72% of cells (n=58/82 cells, 20 plants) with
269   PPBs in *tan1 air9* mutants containing unaltered CFP-TAN1 and YFP-POK1 (Figure 6A, Table 2;
270   Fisher's exact test, P-value = 0.0001). Unaltered CFP-TAN1 fully rescued the *tan1 air9* double
271   mutant (Mills and Rasmussen, 2022), and serves here as a control. Unaltered CFP-TAN1 and YFP-
272   POK1 localized and were maintained at the division site similar to wild type in metaphase (Figure
273   6B, n=13/13), while CFP-TAN1(28-33A) and YFP-POK1 in *tan1 air9* mutants were sometimes
274   absent from the division site in metaphase with only 58% of metaphase cells maintaining both
275   proteins at the division site (n = 11/19 cells, Figure 6F, Table 2). During early telophase, unaltered
276   CFP-TAN1 and YFP-POK1 were always at the division site (n = 14/14, Figure 6C), but CFP-
277   TAN1(28-33A) and YFP-POK1 were maintained at the division site in only 65% of early telophase
278   cells (n = 20/31 cells, Figure 6G, Table 2). Interestingly, YFP-POK1 accumulated in the
279   phragmoplast midline in 26% of early telophase cells (n = 8/31 cells, Table 2) but was not observed
280   in the phragmoplast midline in early telophase cells of plants expressing unaltered CFP-TAN1 (n =
281   0/14 cells, Table 2). During late telophase, when the phragmoplast has contacted the cell cortex in
282   at least one location, CFP-TAN1 and POK1 always localized to the division site (100%, n =63/63
283   cells, Figure 6D). Interestingly, although not observed in earlier stages, YFP-POK1 and CFP-
284   TAN1(28-33A) recruitment to the division site increased to 90% of late telophase cells (n = 53/59
285   cells, Figure 6H). In the remainder of cells, neither CFP-TAN1(28-33) nor YFP-POK1 localized to the
286   division site (3%, n = 2/59), or only CFP-TAN1(28-33) accumulated at the division site (7%, n =
287   4/59 cells). Together, these data suggest that TAN1-POK1 interactions play a critical role in
288   stabilizing them together at the division site. Additionally, it suggests that other, yet unidentified
289   proteins may recruit both TAN1 and POK1 to the division site, particularly during late telophase, in
290   the absence of both AIR9 and TAN1-POK1 interaction.
291
292

Discussion

In *tan1* and *air9* single mutants, POK1 localizes to the division site and there are no discernable division plane defects (Model in Supplementary Figure 6). However, in the *tan1 air9* double mutant, POK1 co-localizes with the PPB but is lost from the division site during metaphase (Model in Figure 7). First, this suggests that TAN1 and AIR9 are not essential for POK1 co-localization with the PPB. Second, it suggests that POK1 is maintained at the division site after PPB disassembly via direct or indirect interactions with TAN1 or AIR9. We provide evidence that TAN1 interacts with POK1 through motifs within the first 132 amino acids of TAN1, as identified using the yeast-two-hybrid system. Alignments of TANGLED1 proteins from representative monocots and dicots, such as *Solanum lycopersium, Oryza sativa, Sorghum bicolor, Zea mays*, and *Brassica napus,* showed that amino acids 28-33 (INKVDK) are highly conserved across plant species (Supplementary Figure 7). Amino acids 30-32 (VDK) are identical and the remaining residues within the motif have similar properties across these plant species. The high degree of conservation suggests that these amino acids are likely important for TAN1 function. When alanine substitutions of these amino acids were introduced into TAN1 and transformed into Arabidopsis *tan1 air9* double mutants, we observed reduced TAN1 and POK1 localization at the division site, as well as defects in phragmoplast positioning. Here we hypothesize that amino acids 28-33 are essential for TAN1 and POK1 interaction in both yeast-two-hybrid and in Arabidopsis. In addition to several reports showing that TAN1 and POK1 interact using the yeast-two-hybrid system (Müller et al., 2006; Rasmussen et al., 2011), bimolecular fluorescence complementation has also been used to show TAN1-POK1 interactions in Arabidopsis protoplasts (Lipka et al., 2014). Alanine substitutions at positions 28-33 of TAN1 may disrupt TAN1-POK1 interaction through misfolding that blocks the POK1 interaction site or by affecting the amino acids that directly mediate POK1 binding. Regardless of the exact mechanism(s) of POK1-TAN1 physical interactions or the possibility that yeast-two-hybrid interactions do not reflect equivalent POK1-TAN1 physical interactions in Arabidopsis, we show that these TAN1 amino acids are involved in mediating TAN1 and POK1 localization to the division site.

We demonstrate that the first region of the TAN1 protein, the first 132 amino acids which primarily accumulates at the division site during telophase (Rasmussen et al., 2011), is both necessary (Mir et al., 2018) and sufficient to largely rescue the *tan1 air9* double mutant (Figure 2). This suggests that $TAN1_{1-132}$ and its recruitment to the division site during telophase is critical for correct division plane orientation in the *tan1 air9* double mutant. Although full length TAN1 localizes to the division site throughout cell division, the ability of $TAN1_{1-132}$ to rescue the *tan1 air9* double mutant, suggests that TAN1, and possibly POK1, localization to the PPB and division site during metaphase may not be required for division site maintenance in Arabidopsis. Indeed, whether the PPB itself is required for division plane positioning has been raised by analysis of a triple mutant in three closely related *TONNEAU RECRUITING MOTIF6,7,8* genes *(trm6,7,8)*. *trm678* mutants, which lacked well defined PPBs, had disrupted POK1 recruitment to the division site but only minor defects in division positioning (Schaefer et al., 2017). However, when amino acids critical for TAN1-POK1 interactions in the yeast-two-hybrid system are disrupted by transforming *TAN1(28-33A)$_{1-132}$-YFP* into the *tan1 air9* double mutant*, root growth and phragmoplast positioning are disrupted.

336   *TAN1(28-33A)$_{1-132}$-YFP* accumulation at the division site during telophase was reduced compared to
337   unaltered *TAN1$_{1-132}$-YFP*. This suggests that TAN1-POK1 interaction promotes, but is not strictly
338   necessary, for TAN1 recruitment to the division site during telophase.
339
340   Full-length TAN1*(28-33A)* localizes to the division site throughout cell division and almost fully
341   rescues the *tan1 air9* double mutant. TAN1, AIR9, and POK1 colocalize at the PPB independently of
342   one another, which may promote the formation of protein complexes required for division site
343   maintenance. Colocalizing with the PPB may provide an opportunity for proteins in close proximity
344   to form stabilizing interactions before PPB disassembly. This suggests that recruitment of TAN1
345   and POK1 to the division site early in cell division may provide another temporally distinct way to
346   promote correct division plane positioning. Phragmoplast positioning defects in TAN1(28-33A)
347   *tan1 air9* plants may be the result of defects in phragmoplast guidance in cells that lacked
348   TAN1(28-33A) and POK1 at the division site in metaphase or early telophase that were not
349   corrected in late telophase.
350
351   The ability of TAN1(28-33A) and POK1 to remain at the division site in some cells after PPB
352   disassembly in the *tan1 air9* double mutant suggests that there are other proteins that interact with
353   TAN1 and/or POK1 that help stabilize them at the division site perhaps via the formation of
354   multiprotein complexes. The pleckstrin homology GAPS, PHGAP1 and PHGAP2 (Stöckle et al.,
355   2016), RANGAP1 (Xu et al., 2008), and IQ67 DOMAIN (IQD)6,7,8 proteins (Kumari et al., 2021) are
356   division site localized proteins that may stabilize TAN1 and POK1 at the division site via their
357   interaction with POK1. PHGAP1, PHGAP2, and RANGAP1 are dependent on POK1 and POK2 for
358   division site recruitment. Like TAN1, RANGAP1 colocalizes with the PPB and remains at the division
359   site throughout cell division (Xu et al., 2008). PHGAP1 and PHGAP2 are uniformly distributed in the
360   cytoplasm and on the plasma membrane in interphase cells and accumulate at the division site
361   during metaphase. These proteins also have their own distinct roles in division site maintenance
362   (Stöckle et al., 2016). PHGAP2 has a likely role in division site establishment by regulating ROP
363   activity (Hwang et al., 2008). RANGAP1 regulation of local RAN-GTP levels has potential roles in
364   microtubule organization and division site identity (Xu et al., 2008). IQD6, IQD7, and IQD8 interact
365   with POK1 and play a role in PPB formation and POK1 recruitment to the division site. *iqd678* triple
366   mutants have PPB formation defects and fail to recruit POK1 to the division site in cells lacking
367   PPBs. However, POK1 localization to the division site in *iqd678* mutants recovers during telophase
368   to wild-type levels (Kumari et al., 2021). We speculate that this IQD6-8 independent recruitment
369   may depend on TAN1. Unlike the PHGAPs and RANGAP1, IQD8 localization to the division site is not
370   dependent on POK1 and POK2. This suggests that IQD6-8 proteins work upstream of POK1 to
371   establish the division site and are important for POK1 recruitment to the division site early in cell
372   division. Although TAN1-POK1 interaction becomes critical for TAN1 and POK1 maintenance at the
373   division site in the absence of AIR9, other division site localized proteins may provide additional
374   stability and help maintain TAN1 and POK1 at the division site.
375
376   How AIR9 stabilizes POK1 at the division site in the absence of TAN1 is less clear. There is no
377   information about whether POK1 and AIR9 interact directly with one another. Additionally, AIR9
378   localization, in contrast to TAN1 localization, is intermittent at the division site. When expressed in

8

379   tobacco Bright Yellow2 (BY2) cells, AIR9 colocalizes with the PPB but is then lost from the division
380   site until late telophase when the phragmoplast contacts the cortex (Buschmann et al., 2006). In
381   Arabidopsis, AIR9 may localize to the division site during metaphase or telophase, but it is difficult
382   to observe because AIR9 also strongly colocalizes with cortical microtubules which may obscure
383   AIR9 localization in nearby cells (Buschmann et al., 2015). Rather than directly interacting with
384   POK1, AIR9 may recruit other proteins to the division site during preprophase that help maintain
385   POK1 at the division site in the absence of TAN1. One potential candidate is the kinesin-like
386   calmodulin binding protein, KCBP, which interacts with AIR9 (Buschmann et al., 2015). KCBP is a
387   minus-end-directed kinesin (Song et al., 1997) that localizes to the division site in Arabidopsis and
388   moss (Miki et al., 2014; Buschmann et al., 2015). We speculate that other TAN1, AIR9, and POK1
389   interacting proteins that have not been identified yet may be key for TAN1-POK1 division site
390   maintenance.
391
392   POK1 and POK2 have roles in phragmoplast guidance, but POK2 also has a role in phragmoplast
393   dynamics (Lipka et al., 2014; Herrmann et al., 2018). Although POK1 does not frequently
394   accumulate in the phragmoplast midline in wild-type cells, POK2 showed striking dual localization
395   to both the phragmoplast midline and the division site. Localization of POK2 to the phragmoplast
396   midline required the N-terminal motor domain, while the C-terminal region was localized to the
397   division site (Herrmann et al., 2018). Our hypothesis is that the "default" location of both POK1 and
398   POK2 is at microtubule plus-ends at the phragmoplast midline, based on likely or confirmed plus-
399   end directed motor activity (Chugh et al., 2018). Interactions with division site localized proteins,
400   such as TAN1 and AIR9, may stabilize or recruit POK1 and POK2 at the division site away from the
401   phragmoplast midline.
402
403   We demonstrate that AIR9 and TAN1 function redundantly to maintain POK1 at the division site to
404   ensure correct cell wall placement. In the absence of AIR9, our data suggests that TAN1-POK1
405   interaction promotes, but is not required for, the maintenance of both proteins at the division site
406   and disrupting this interaction partially disrupts their localization to the division site. This also
407   suggests that other TAN1, POK1, and AIR9 interacting proteins are involved with stabilizing TAN1
408   and POK1 at the division site.
409
410
411   **Materials and methods**
412   Growth conditions, genotyping mutants, and root length measurements
413   Arabidopsis seedlings were grown on ½ strength Murashige and Skoog (MS) media (MP
414   Biomedicals; Murashige and Skoog, 1962) containing 0.5 g/L MES (Fisher Scientific), pH 5.7, and
415   0.8% agar (Fisher Scientific). Seeds sown on plates were first stratified in the dark at 4°C for 2 to 5
416   days then grown vertically in a growth chamber (Percival) with 16/8-h light/dark cycles and
417   temperature set to 22°C. For root length experiments, *tan1 air9* transgenic T3 lines expressing
418   *p35S:TAN1-YFP, 35S:TAN1$_{1-132}$-YFP, 35S:TAN1(28-33A)$_{1-132}$-YFP*, or *35S:YFP-TAN1(28-33A)* were
419   grown vertically, the plates were scanned (Epson) and root lengths were measured using FIJI
420   (ImageJ, http:/ /fiji.sc/) after 8 days. Untransformed *tan1 air9* double mutants and *air9* single
421   mutants were grown alongside the double mutant seeds expressing the TAN1 constructs in equal

422   numbers on the same plates to ensure plants were grown under the same conditions. After plates
423   were scanned, seedlings were screened by confocal microscopy to identify seedlings expressing
424   YFP translational fusion transgenes and CFP-TUBULIN, if present in the transgenic lines. At least 3
425   biological replicates, grown on separate plates on separate days, and at least 28 plants of each
426   genotype total across all replicates were analyzed for each root growth experiment. Welch's t-test
427   was used to identify whether there were statistically significant differences between replicates
428   before pooling the replicates for analysis. Root lengths were then plotted using Prism (GraphPad).
429   Statistical analysis of root length was performed with Prism (GraphPad) using t-test with Welch's
430   correction. Welch's t-test (unequal variance t-test) is used to test the hypothesis that two
431   populations have equal means. Unlike the Student's t-test, Welch's t-test is often used when two
432   samples have unequal variances or sample sizes. This test was used due to the unequal sample sizes
433   because the plants examined were often segregating for multiple transgenes and had lower sample
434   sizes than control plants such as *air9* single mutants and *tan1 air9* double mutants which either
435   lacked transgenes or were segregating fewer transgenes.
436
437   YFP translational fusion TAN1 constructs were analyzed in *csh-tan* (*TAN1,* AT3G05330) *air9-31*
438   (*AIR9*, AT2G34680) double mutants in *Landsberg erecta (Ler)* unless otherwise specified. The
439   *pPOK1:YFP-POK1* transgene in Columbia, a kind gift from Sabine Müller (Lipka et al., 2014), was
440   crossed into the *tan-mad* and *air9-5* Columbia/Wassilewskija double mutant previously described
441   (Mir et al., 2018). *tan-mad* and *air9-5* mutants were genotyped with primers ATRP and ATLP (to
442   identify wild-type *TAN1*), JL202 and ATLP (to identify T-DNA insertion in *TAN1*), AIR9-5RP and
443   AIR9-5LP (to identify wild-type *AIR9*), and LBb1.3 and AIR9RP (to identify T-DNA insertion in *AIR9*)
444   and by observation of the *tan1 air9* double mutant phenotype (Supplementary Table 1).
445
446   <u>Generation of Transgenic Lines</u>
447   *Agrobacterium tumefaciens*-mediated floral dip transformation was used as described (Clough and
448   Bent, 1999). *csh-tan air9-31* double mutants were used for all floral dip transformations unless
449   otherwise specified. Transgenic plants were selected on 15 μg/mL glufosinate (Finale; Bayer) and
450   screened by microscopy before being transferred to soil and selfed. *CFP-TUBULIN* was crossed into
451   3$5S:TAN1(28-33A)_{1-132}$-YFP *tan1 air9* plants using tan*1 air9 CFP-TUBULIN* plants (Mir et al., 2018)
452   and progeny were subsequently screened by microscopy for CFP and YFP signal. *csh-tan1 air9-31*
453   double mutants were confirmed by genotyping with primers ATLP and AtTAN 733-CDS Rw (to
454   identify TAN1 wild-type), AtTAN 733-CDS Rw and Ds5-4 (to identify T-DNA insertion in *TAN1*),
455   AIR9_cDNA 2230 F and AIR9 gnm7511 R (to identify *AIR9* wild-type), and AIR9 gnm7511 R and
456   Ds5-4 (to identify T-DNA insertion in *AIR9*).
457
458   Columbia expressing the microtubule marker *UBQ10:mScarlet-MAP4* (Pan et al., 2020), a kind gift
459   from Xue Pan and Zhenbiao Yang (UCR), was crossed to *tan-mad* and *air9-5*
460   Columbia/Wassilewskija double mutants expressing *pPOK1:YFP-POK1*. Progeny were screened for
461   mScarlet-MAP4 and YFP-POK1 by confocal microscopy and then selfed to recover *air9-5* single
462   mutants, *tanmad* single mutants, and *air9-5 tan-mad* double mutants expressing *mScarlet-MAP4*
463   and *YFP-POK1*.
464

10

465 *pTAN1:CFP-TAN1* and *pTAN1:CFP-TAN1(28-33A)* were introduced into *air9-5 tan-mad* double
466 mutants expressing *mScarlet-MAP4* and *YFP-POK1* by *Agrobacterium tumefaciens*-mediated floral
467 dip transformation. *pTAN1:CFP-TAN1* and *pTAN1:CFP-TAN1(28-33A)* transformants were selected
468 on 100μg/mL gentamicin (Fisher Scientific) and the presence of mScarlet-MAP4, YFP-POK1, and
469 either CFP-TAN1 or CFP-TAN1(28-33A) was confirmed by confocal microscopy. 4 independent
470 transformed lines for *pTAN:CFP-TAN1(28-33A)* and 3 independent transformed lines for unaltered
471 *pTAN:CFP-TAN1* were examined for division site localization cell counts.

472

473 <u>Plasmid Construction</u>
474 *TAN1$_{1-132}$-YFP* coding sequences were subcloned by EcoRI and BamHI double digestion from the
475 plasmid *pEZRK-LNY-TAN1$_{1-132}$-YFP* described previously (Rasmussen et al., 2011) into *pEZT-NL*
476 vector (a kind gift from David Ehrhardt, Carnegie Institute, Stanford University) and selected with
477 glufosinate (Finale; Bayer). The CFP-TUBULIN (CFP-TUA6) vector was previously described, a kind
478 gift from Viktor Kirik (Kirik et al., 2007).

479

480 Six amino acid alanine substitutions were generated using overlapping PCR (primers in
481 Supplementary Table 1) beginning at amino acid 10 of TAN1$_{1-132}$. *TAN1$_{1-132}$-YFP* coding sequence
482 from plasmids described previously was used as the PCR template (Rasmussen et al., 2011).
483 *TAN1(28-33A)$_{1-132}$-YFP* was subcloned by EcoRI BamHI double digestion into pEZT-NL. To generate
484 *YFP-TAN1(28-33A)*, alanine substitutions were first introduced into G22672 (TAN1 cDNA in
485 pENTR223, from the Arabidopsis Biological Resource Center) using overlapping PCR with the same
486 primers to generate *TAN1(28-33A)*. Gateway LR reaction (Fisher Scientific) was then used to
487 subclone *TAN1(28-33A)* into pEarley104 (Earley et al., 2006).

488

489 *pTAN:CFP-TAN1(28-33A)* was generated using overlapping PCR. The TANGLED1 native promoter
490 was amplified from *Np:AtTAN-YFP (Walker et al., 2007)* using the primers NpTANSacIFor and
491 NpTANceruleanRev. Cerulean was amplified from the Cerulean CDS in pDONR221P4r/P3r using
492 the primers NpTANceruleanFor and CeruleanpEarleyRev. TAN1(28-33A) in pEarley104 was
493 amplified using CeruleanpEarleyFor and pEarleyOCSPstIRev. TANGLED1 native promoter,
494 Cerulean, and TAN1(28-33A) were then combined using overlapping PCR using NpTANSacI and
495 pEarleyOCSPstIRev. *pTAN:CFP-TAN1(28-33A)* was then subcloned into pJHA212G, a kind gift of
496 Meng Chen (UCR), using SacI and PstI double digest. pTAN:CFP-TAN1 was generated the same way
497 as pTAN:CFP-TAN1(28-33A) except unaltered TAN1 in pEarley104 was amplified using
498 CeruleanpEarleyFor and pEarleyOCSPstIRev.

499

500 <u>Microscopy</u>
501 An inverted Ti Eclipse (Nikon) with motorized stage (ASI Piezo) and spinning-disk confocal
502 microscope (Yokogawa W1) built by Solamere Technology was used with Micromanager software
503 (micromanager.org). Solid-state lasers (Obis) and emission filters (Chroma Technology) were used.
504 For CFP translational fusions excitation 445, emission 480/40 was used; YFP translational fusions
505 excitation 514, emission 540/30; and propidium iodide (PI), Alexa-568 goat anti-mouse antibody,
506 and mScarlet-MAP4 excitation 561, emission 620/60 were used. The 20x objective has 0.75
507 numerical aperture and the 60x objective has 1.2 numerical aperture which was used with

11

508 perfluorocarbon immersion liquid (RIAAA-6788 Cargille). Excitation spectra for mScarlet-MAP4
509 and YFP-POK1 partially overlapped, which resulted in faint bleed through signal in the YFP channel
510 for some dense microtubule structures (e.g. spindles and phragmoplasts). YFP-POK1 colocalization
511 with PPBs was carefully determined based on distinct YFP-POK1 signal and the presence of
512 cytosolic YFP-POK1.
513
514 The ratio of the division site versus cytosolic fluorescence intensity was determined by taking the
515 median YFP fluorescence intensity from the center Z-stack of individual cells with PPBs or
516 phragmoplasts. For each cell the median fluorescence intensity was measured for two cytosolic
517 areas and the division site on each side of the cell using circles with areas of 0.875 μm^2. The sum of
518 the median intensity at the division site on each side was then divided by the sum of the median
519 intensity of the two cytosolic areas to calculate the ratio of the division site versus cytosolic
520 fluorescence intensity. Fluorescence intensities were measured in FIJI. All plants used for this
521 analysis were grown on the same day and imaged using identical conditions, and at least 5 plants of
522 each genotype were examined.
523
524 <u>Measurements of PPB and phragmoplast angles and cell file rotation</u>
525 At least 3 biological replicates, grown on separate plates on separate days, composed of at least 15
526 plants per genotype for PPB measurements and at least 8 plants per genotype for phragmoplast
527 measurements were used to gather angle data. 8-day-old seedlings were stained with 10 μM PI for
528 1 minute and then destained in distilled water before imaging by confocal microscopy using a 20x
529 or 60x objective. PPB and phragmoplast angles were measured using FIJI. The angle was measured
530 between the left-hand cell wall and the orientation of the PPB or phragmoplast in the root tips of
531 *tan1 air9* double mutants expressing *CFP-TUBULIN* or immunostained microtubules (described in
532 the next section). Cell file rotation was examined by measuring from the left-hand side of the
533 transverse cell wall relative to the long axis of the root in images of the differentiation zone stained
534 with PI. The differentiation zone was identified by the presence of root hairs. Prism (GraphPad) and
535 Excel (Microsoft Office) were used to perform statistical analyses and to plot data. F-test was used
536 to compare normally distributed variances (PPB and phragmoplast angles) and Levene's test was
537 used to compare non-normally distributed variances (cell file rotation angle measurements). *tan1*
538 *air9* double mutants have non-normally distributed cell file twisting because the roots tend to twist
539 to the left (Mir et al., 2018). Genotypes across biological replicates were compared to ensure there
540 was no statistically significant difference between them before pooling data.
541
542 <u>Immunostaining</u>
543 *air9, tan1 air9 p35S:TAN1-YFP, tan1 air9 35S:YFP-TAN1(28-33A),* and untransformed *tan1 air9*
544 plants were stratified and then grown vertically on ½ MS plates in a growth chamber at 22°C with a
545 16/8-h light/dark cycle for 8 days. The seedlings were screened by microscopy for YFP and then
546 fixed and processed for immunofluorescence microscopy using a 1:2000 dilution of monoclonal
547 anti-α-tubulin B-5-1-2 antibody (Life Technologies; 32-2500) followed by 1:2000 dilution of Alexa-
548 568 goat anti-mouse antibody (Thermo Fisher; A-11004) as described previously (Sugimoto et al.,
549 2000).
550

Yeast-two-hybrid

Six alanine substitutions were generated using overlapping PCR and TAN1 coding sequence in pEZRK-LNY-*TAN1*$_{1-132}$-*YFP* as a template beginning at amino acid 10 of TAN1 and continuing through amino acid 123 according to (Russell and Sambrook, 2001). All except amino acids substitutions for 64-69 and 106-111 were cloned into pAS vector (Fan et al., 1997) using EcoRI BamHI double digestion. pBD-TAN1(28-33A) was generated by using primers Ala_05_FOR and Ala_05_REV to perform DpnI mediated site-directed mutagenesis by PCR (Fisher and Pei, 1997). pBD-TAN1 (Walker et al., 2007), and pAS-*TAN1*$_{1-132}$ (Rasmussen et al., 2011) were used as positive controls, while pAD-MUT was used as a negative control for testing interaction with pAD-POK1 (Müller et al., 2006). *pAD-POK1* and *pAS-TAN1*$_{1-132}$ constructs were co-transformed into yeast strain YRG2 according to manufacturer instructions (Stragene). Positive yeast-two-hybrid interaction was determined by the presence of growth on plates cultured at 30°C lacking histidine after 3 days. Plates were then scanned (Epson).

Figure 1: TAN1 and AIR9 together promote POK1 maintenance at the division site. YFP-POK1 localization in Col-0 wild-type plants, *tan1* single mutants, *air9* single mutants, and *tan1 air9* double mutants expressing *UBQ10:mScarlet-MAP4* to mark microtubules and *pPOK1:YFP-POK1*. Scale bars = 10 μm. A-C) YFP-POK1 localization in Col-0 wild-type plants, N = 15 plants. A) YFP-POK1 localization during preprophase/prophase. In 71% of cells (50/70) YFP-POK1 colocalized with the PPB. B) YFP-POK1 was observed to be maintained at the division site in metaphase and anaphase cells in Col-0 plants (n = 13/13 metaphase cells, n = 3/3 anaphase cells). C) YFP-POK1 remains clearly visible at the division site in Col-0 telophase cells (n = 31/31 cells). D-F) YFP-POK1 localization in *tan1 air9* double mutant plants, N = 19 plants. D) YFP-POK1 localization during preprophase/prophase. In 50% of cells (27/54) YFP-POK1 colocalized with the PPB. E) YFP-POK1 was observed to be lost from the division site upon entry into metaphase (n = 0/21 cells) and was absent in anaphase cells (n = 0/4 cells). F) In *tan1 air9* telophase cells YFP-POK1 was absent from the division site and accumulated in the phragmoplast midline (n = 34/44 cells). G-I) YFP-POK1 localization in *tan1* single mutants, N = 17 plants. G) YFP-POK1 localization during preprophase/prophase. In 64% of cells (54/85) YFP-POK1 colocalized with the PPB. H) YFP-POK1 was observed to be maintained at the division site in metaphase and anaphase cells in *tan1* plants (n = 17/17 metaphase cells, n = 6/6 anaphase cells). I) YFP-POK1 remains clearly visible at the division site in *tan1* telophase cells (n = 27/27 cells). J-L) YFP-POK1 localization in *air9* single mutant plants (N = 15 plants). J) YFP-POK1 localization during preprophase/prophase. In 64% of cells (46/72) YFP-POK1 colocalized with the PPB. K) YFP-POK1 was maintained at the division site in metaphase and anaphase cells in *air9* plants (n = 24/24 metaphase cells, n = 4/4 anaphase cells). L) YFP-POK1 remains clearly visible at the division site in *air9* telophase cells (n = 40/40 cells).

14
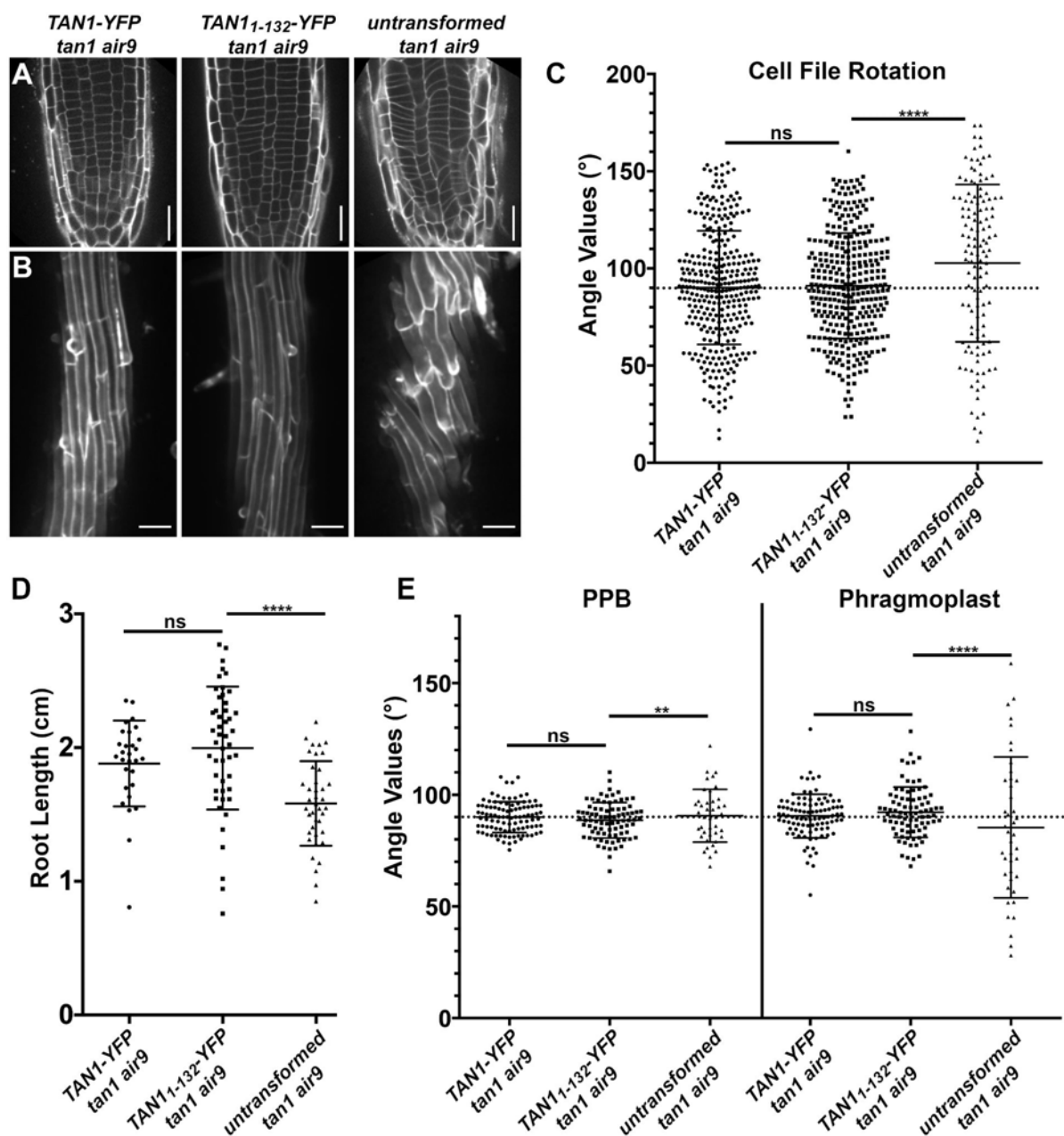
Figure 2. *p35S:TAN1$_{1-132}$-YFP* rescues Arabidopsis *tan1 air9* double mutant phenotypes. A) Cell walls stained with propidium iodide (PI) of *tan1 air9* double mutant root tips expressing *p35S:TAN1-YFP* (left), *p35S:TAN1$_{1-132}$-YFP* (middle), and untransformed *tan1 air9* double mutants (right). Bars = 25 μm. B) Maximum projections of 10 1-μm Z-stacks of PI-stained differentiation zone root cell walls. Scale bars = 50 μm. C) Cell file rotation angles of *tan1 air9* double mutants expressing *p35S:TAN1-YFP* (left), *p35S:TAN1$_{1-132}$-YFP* (middle) and untransformed plants (right), n > 13 plants for each genotype. Each dot represents an angle measured from the left side of the long axis of the root to the transverse cell wall. Angle variances were compared with Levene's test due to non-normal distribution. D) Root length measurements from 8 days after stratification of *tan1 air9* double mutants expressing p*35S:TAN1-YFP* (left), *p35S:TAN1$_{1-132}$-YFP* (middle) and untransformed

15

610   plants (right), n > 28 plants for each genotype, compared by two-tailed t-test with Welch's

611   correction. E) PPB and phragmoplast angle measurements in *tan1 air9* double mutant cells

612   expressing p*35S:TAN1-YFP* (left), *p35S:TAN1₁₋₁₃₂-YFP* (middle) and untransformed plants (right), n

613   > 20 plants for each genotype. Angle variations compared with F-test. ns indicates not significant,

614   ** P-value <0.01, **** P-value <0.0001.

615
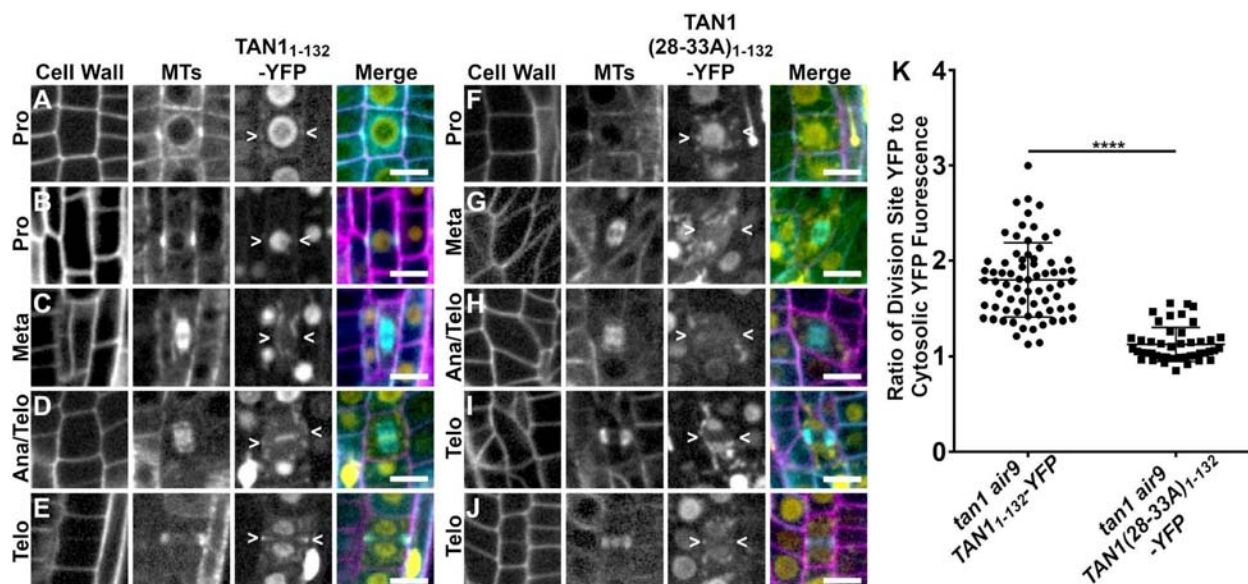
**Figure 3: Division site localization during telophase is common for TAN1$_{1-132}$-YFP but rare for TAN1(28-33A)$_{1-132}$-YFP in *tan1 air9* double mutants.** A-E) Propidium iodide stained *tan1 air9* plants expressing *p35S:TAN1$_{1-132}$-YFP* during mitosis (n = 29 plants). The division site is indicated by arrowheads in the YFP panels. Scale bars = 10 μm. A) Rare prophase division site accumulation of TAN1$_{1-132}$-YFP, (10%, n = 9/89 cells), (B) common prophase TAN1$_{1-132}$-YFP nuclear accumulation without division site localization (90%, n = 80/89 cells), (C) no specific TAN1$_{1-132}$-YFP division site accumulation in metaphase (100%, n = 28/28 cells), (D) faint TAN1$_{1-132}$-YFP division site accumulation accompanied by midline accumulation in late anaphase/early telophase (80%, n = 16/20 cells) and E) TAN1$_{1-132}$-YFP division site accumulation during telophase (100%, n = 58/58 cells). F-H) *tan1 air9* plants expressing p*35S:TAN1(28-33A)$_{1-132}$-YFP* during mitosis (n = 13 plants). The division site is indicated by arrowheads in the YFP panels. F) No specific TAN1(28-33A)$_{1-132}$-YFP prophase division site accumulation during prophase (100%, n = 20/20 cells), (G) no specific TAN1(28-33A)$_{1-132}$-YFP division site accumulation during metaphase (100%, n = 12/12 cells), (H) no TAN1(28-33A)$_{1-132}$-YFP division site or midline accumulation in late anaphase/early telophase (100%, n = 8/8 cells), (I) no specific TAN1(28-33A)$_{1-132}$-YFP division site accumulation during telophase (68%, n = 15/22 cells) and (J) faint TAN1(28-33A)$_{1-132}$-YFP division site accumulation during telophase (32%, n = 7/22 cells). K) Ratio of TAN1$_{1-132}$-YFP (left) or TAN1(28-33A)$_{1-132}$-YFP (right) fluorescence at the division site to cytosolic fluorescence from *tan1 air9* plants expressing *p35S:TAN1$_{1-132}$-YFP* or *p35S:TAN1(28-33A)$_{1-132}$-YFP* during telophase, n >23 plants for each genotype. Asterisks indicate a significant difference as determined by Mann-Whitney U test, P-value <0.0001.

17
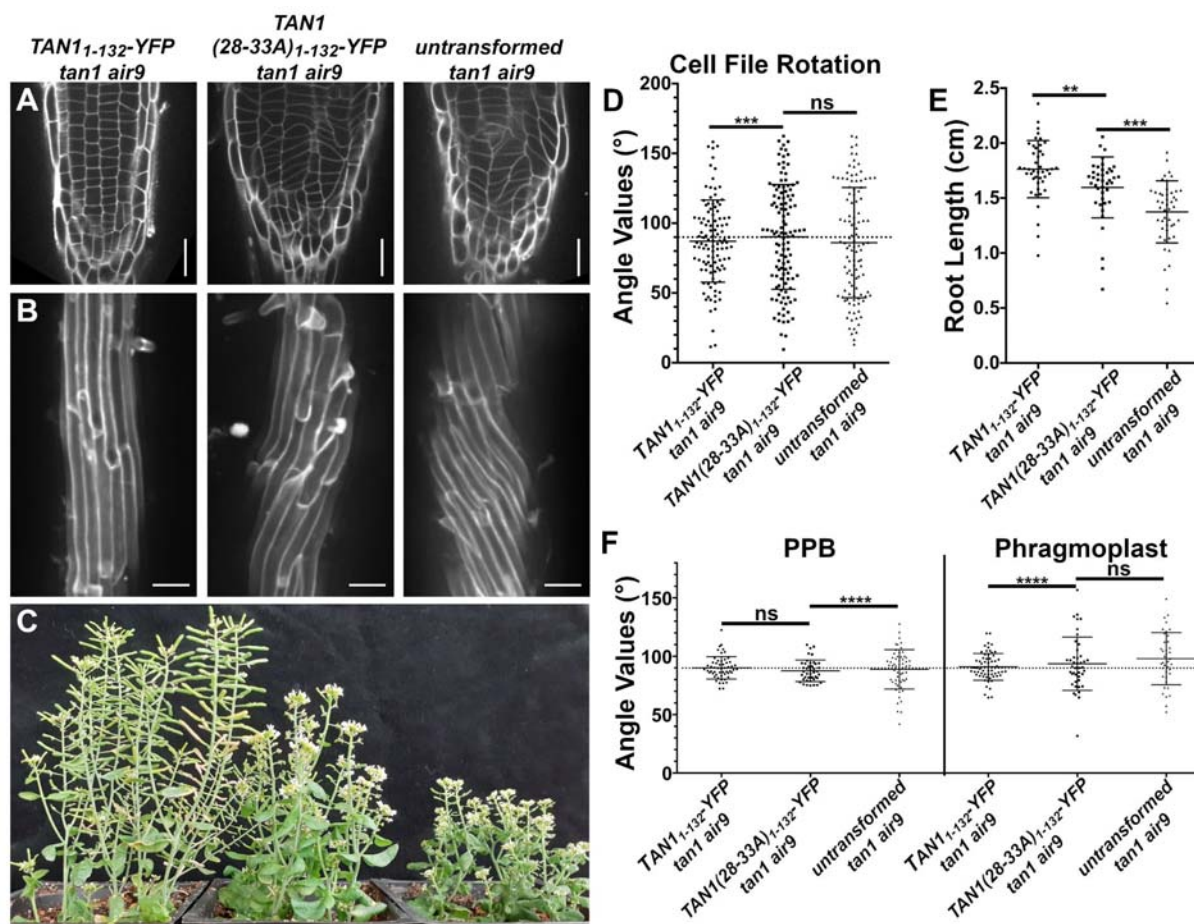
Figure 4: *p35S:TAN1(28-33A)$_{1-132}$-YFP* partially rescues *tan1 air9* double mutant phenotypes.
A) Cell walls of Arabidopsis *tan1 air9* double mutant root tips stained with propidium iodide (PI) of plants expressing *p35S:TAN1$_{1-132}$-YFP* (left), *p35S:TAN1(28-33A)$_{1-132}$-YFP* (middle), and untransformed *tan1 air9* double mutants (right). Scale bars = 25 μm. B) Maximum projections of 10 1-μm Z-stacks of PI-stained differentiation zone root cell walls. Scale bars = 50 μm. C) 58-day old *tan1 air9* double mutants expressing *p35S:TAN1$_{1-132}$-YFP* (left), *p35S:TAN1(28-33A)$_{1-132}$-YFP* (middle), and untransformed *tan1 air9* double mutants (right). D) Cell file rotation angles of *tan1 air9* double mutants expressing *p35S:TAN1$_{1-132}$-YFP* (left), *p35S:TAN1(28-33A)$_{1-132}$-YFP* (middle), and untransformed *tan1 air9* double mutants (right) n > 27 plants for each genotype. Variances were compared with Levene's test. E) Root length measurements from 8 days after stratification of *tan1 air9* double mutants expressing *p35S:TAN1$_{1-132}$-YFP* (left), *p35S:TAN1(28-33A)$_{1-132}$-YFP* (middle), and untransformed *tan1 air9* double mutants (right), n > 40 plants for each genotype, two-tailed t-test with Welch's correction. F) PPB and phragmoplast angle measurements in dividing root cells of *tan1 air9* double mutants expressing *p35S:TAN1$_{1-132}$-YFP* (left), *p35S:TAN1(28-33A)$_{1-132}$-YFP* (middle), and untransformed plants (right), n > 17 plants for each genotype. Angle variance compared with F-test. ns indicates not significant, ** P-value <0.01, *** P-value <0.001, **** P-value <0.0001.

18
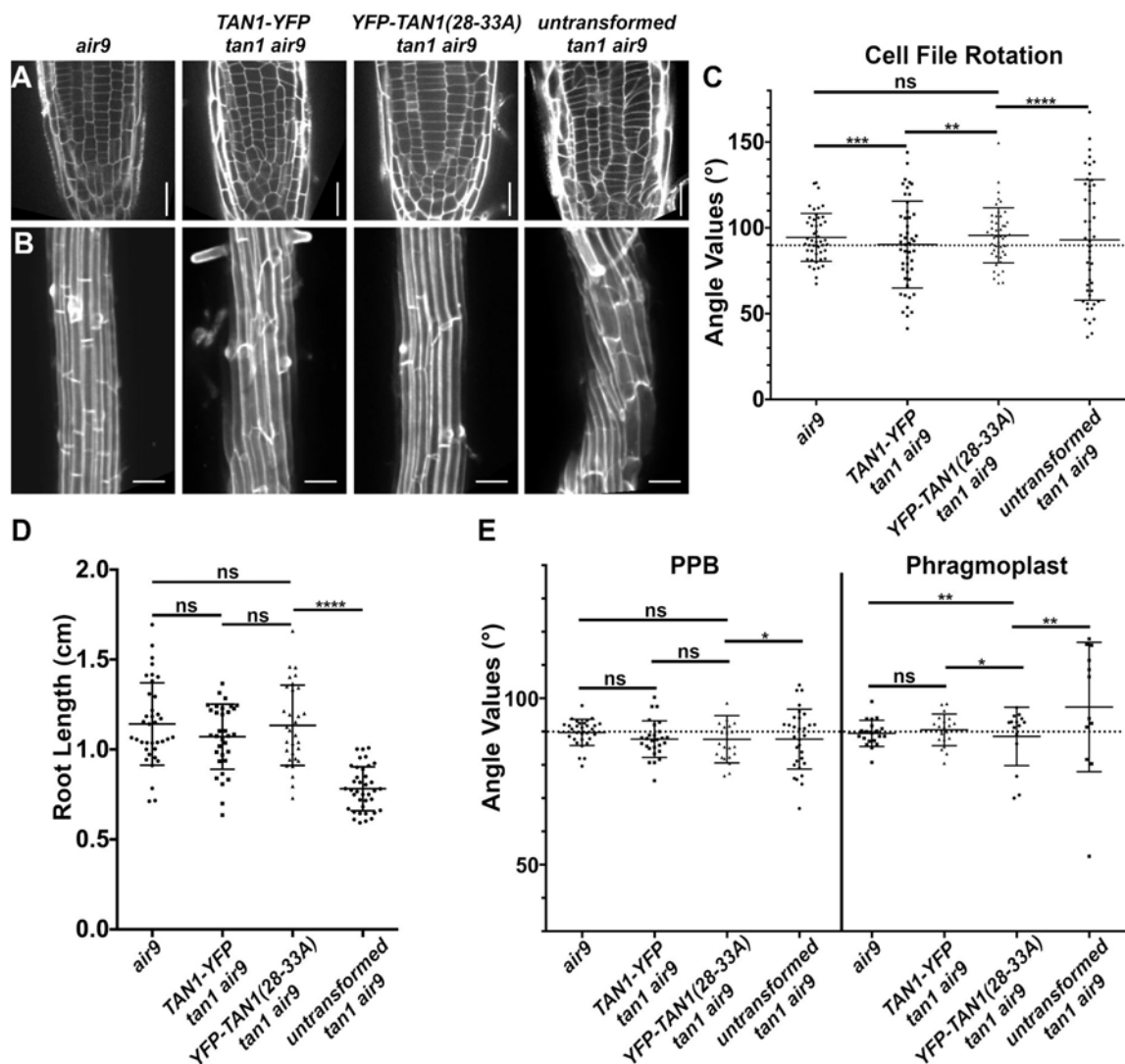
Figure 5: Full length *TAN1* with alanine substitutions replacing amino acids 28 to 33 (*p35S:YFP-TAN1(28-33A)*) mostly rescues the t*an1 air9* double mutant. A) Propidium iodide stained root tips of an *air9* single mutant (left) and *tan1 air9* double mutants expressing *p35S:TAN1-YFP* (center left) or *p35S:YFP-TAN1(28-33A)* (center right), and an untransformed *tan1 air9* plant (right). Scale bars = 25 μm. B) Maximum projections of 10 1-μm Z-stacks of PI-stained cell walls in the root differentiation zone. Scale bars = 50 μm. C) Cell file rotation angles of *air9* single mutants (left), *tan1 air9* double mutant plants expressing p*35S:TAN1-YFP* (center left) or *p35S:YFP-TAN1(28-33A)* (center right), and untransformed *tan1 air9* plants (right), n > 9 plants for each genotype. Variances were compared with Levene's test. D) Root length measurements from 8 days after stratification of *air9* single mutants (left) and *tan1 air9* double mutants expressing *p35S:TAN1-YFP* (center left) or *p35S:YFP-TAN1(28-33A)* (center right), and untransformed *tan1 air9* plants (right), n > 30 plants of each genotype, compared by two-tailed t-test with Welch's correction. E) PPB and phragmoplast angle measurements in dividing root cells of *air9* single mutants (left) and *tan1 air9* double mutant plants expressing *p35S:TAN1-YFP* (center left) or *p35S:YFP-TAN1(28-33A)* (center right), and untransformed *tan1 air9* plants (right), PPB

19

675 measurements n > 15 plants for each genotype; phragmoplast measurements n > 8 plants for each
676 genotype. Angle variance compared with F-test. ns indicates not significant, * P-value <0.05, ** P-
677 value <0.01, *** P-value <0.001, **** P-value <0.0001.

678
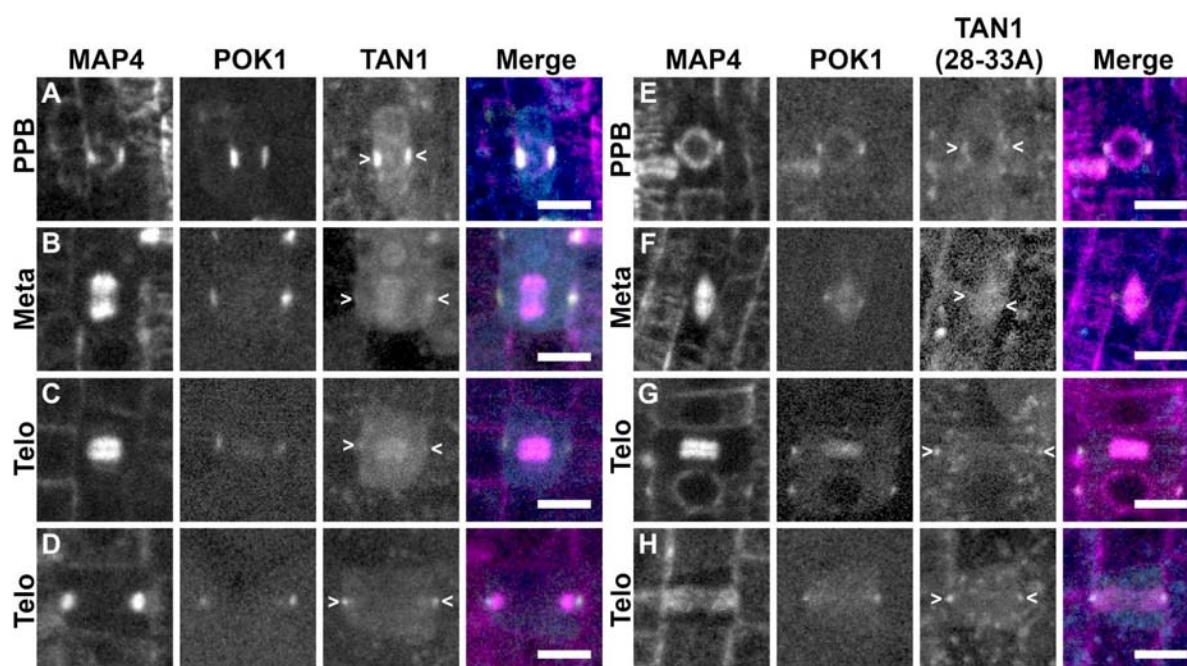
679
680
Figure 6: CFP-TAN1(28-33A) and YFP-POK1 exhibit impaired recruitment to the division site in the *tan1 air9* double mutant. YFP-POK1 localization in *tan1 air9* double mutants expressing *UBQ10:mScarlet-MAP4* and either (A-D) *pTAN1:CFP-TAN1* (n = 20 plants) or (E-I) *pTAN1:CFP-TAN1(28-33A)* (n = 22 plants). Maximum projections of 3 1-µm Z-stacks. Scale bars = 10 µm. Some bleed through from the mScarlet channel can be seen in the YFP-POK1 panels. A) YFP-POK1 and CFP-TAN1 colocalized with the PPB in 72% of cells (n = 59/82 cells). B) YFP-POK1 and CFP-TAN1 were maintained at the division site in metaphase 13/13 and anaphase 4/4 cells. C) YFP-POK1 and CFP-TAN1 were maintained at the division site in all early telophase cells (n = 14/14 cells) and late telophase (n = 63/63 cells). E) YFP-POK1 and CFP-TAN1(28-33A) colocalized with the PPB in 41% of cells (n = 32/79 cells). F) YFP-POK1 and CFP-TAN1(28-33A) were maintained at the division site in 58% of metaphase cells (n = 11/19 cells). CFP-TAN1(28-33A) was faint at the division site. G) Both YFP-POK1 and CFP-TAN1(28-33A) were observed at the division site in 65% of early telophase cells (n = 20/31 cells). H) YFP-POK1 and CFP-TAN1(28-33A) were recruited to the division site in 90% of late telophase cells (n = 53/59 cells). Some late telophase cells were observed to have CFP-TAN1(28-33A) but not YFP-POK1 at the division site (7%, n = 4/59 cells) or neither CFP-TAN1(28-33A) or YFP-POK1 at the division site (3% n = 2/59 cells).
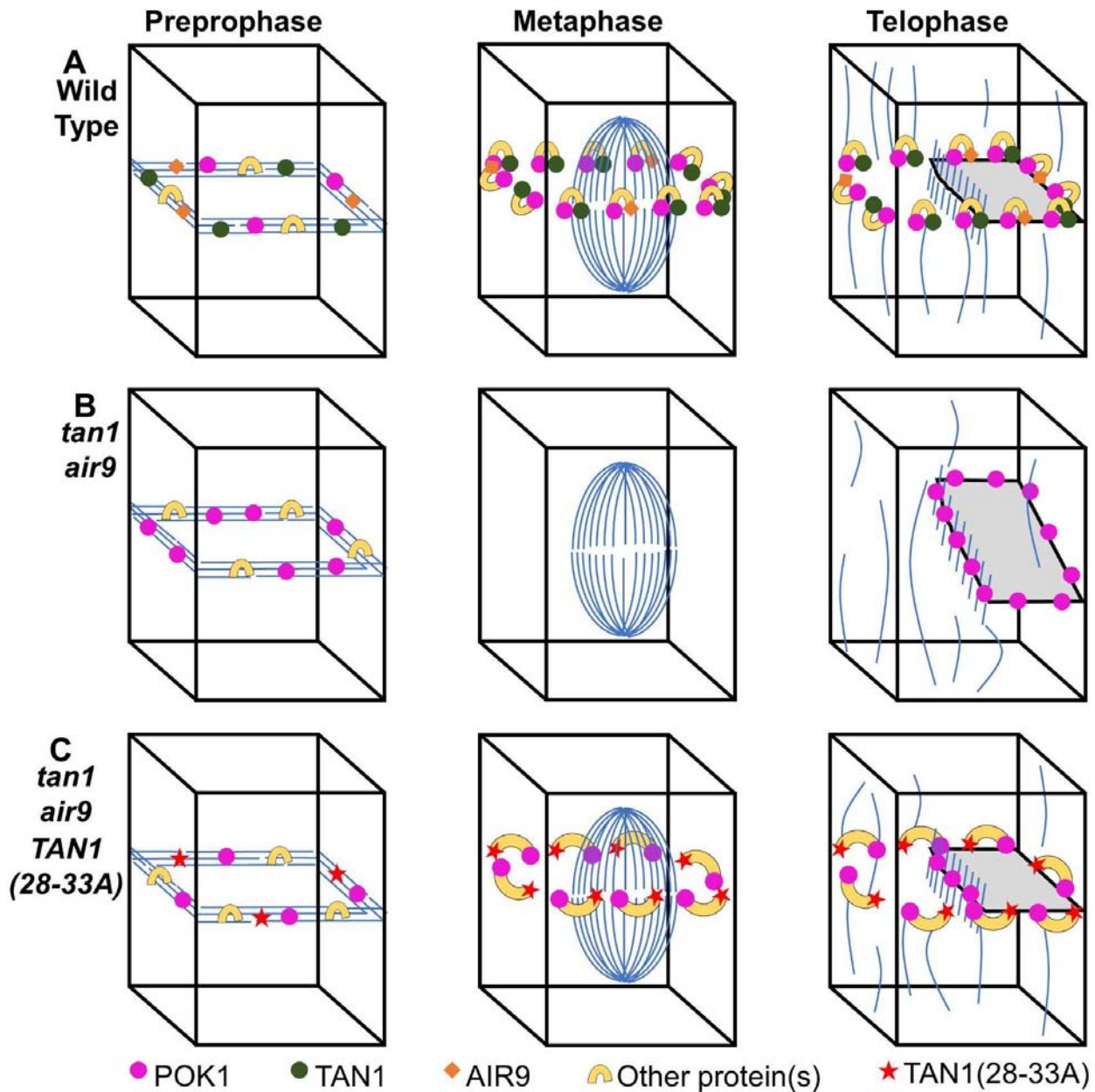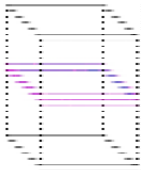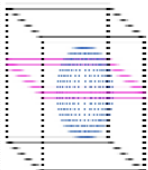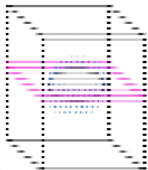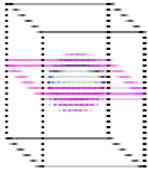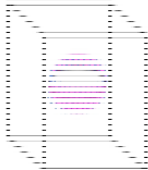
Figure 7: A speculative model on TAN1, AIR9, and POK1 interactions to ensure correct division plane orientation. A) In wild-type (WT) cells, AIR9, TAN1, and POK1 are recruited independently of one another to the PPB. Interaction between TAN1 and POK1 maintain both proteins at the division site through telophase, with AIR9 being re-recruited to the division site in late telophase. B) In the *tan1 air9* double mutant, TAN1, AIR9, and potential AIR9/POK1 interacting proteins are recruited to the PPB. Upon disassembly of the PPB, POK1 is lost from the division site and during telophase aberrantly accumulates in the phragmoplast midline. Due to the loss of TAN1 and POK1 from the division site, the phragmoplast is not guided to the location defined by the PPB.
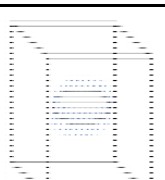
22
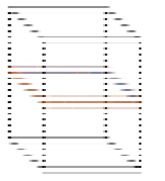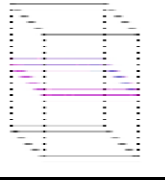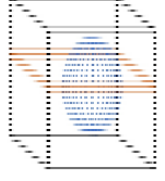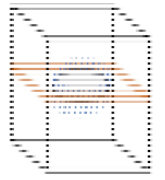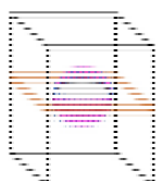
707   C) In *tan1 air9* double mutants expressing *TAN1(28-33A)*, TAN1(28-33A) and POK1 are recruited to
708   the PPB independently of one another. POK1 and TAN1(28-33A) are partially maintained in some
709   metaphase and early telophase cells possibly by interactions with other proteins. However, due to
710   the inability of TAN1(28-33A) and POK1 to interact with one another, both proteins are not
711   efficiently maintained at the division site. The majority (90%) of late telophase cells contain both
712   POK1 and TAN1(28-33A) at the division site. Late recruitment of POK1 and TAN1(28-33A) may
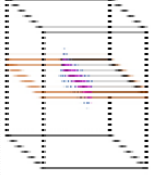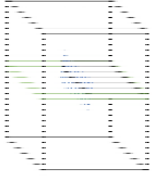713   help guide the phragmoplast to the correct division site in a majority of cells.

Table 1. YFP-POK1 division site and phragmoplast midline accumulation in wild-type, *tan1*, *air9,* and *tan1 air9* double mutant plants. Statistically significant differences were determined using Fisher's exact test with Bonferroni correction - for 4 sample types, P < 0.0125 is significant. P-values are in parentheses. Stars indicate significant differences; ns indicates not significant. Magenta represents YFP-POK1, blue represents microtubules, and light gray represents the cell plate in schematics.

Schematic	Description	Wild-type, N = 15 plants	*tan1 air9*, N =19 plants	*tan1*, N =17 plants	*air9*, N = 15 plants
	PPB, POK1 at the division site	71%, n = 50/70	50%, n = 27/54 (p = 0.0165, ns with Bonferroni correction)	64%, n = 54/85 (ns)	64%, n = 46/72 (ns)
	Metaphase, POK1 at the division site	100%, n = 13/13	0%, n = 0/21*** (p < 0.00001)	100%, n = 17/17 (ns)	100%, n = 24/24 (ns)
	Telophase, POK1 at the division site only	87%, n = 27/31	0%, n= 0/44 ***(p < 0.00001)	56%, n = 15/27** (p = 0.0094)	90%, n = 36/40 (ns)
	Telophase, POK1 at the division site and in the phragmoplast midline	13%, n = 4/31	0%, n = 0/44 (p = 0.0259, ns with Bonferroni correction	44%, n = 12/27** (p = 0.0094)	10%, n = 4/40 (ns)
	Telophase, POK1 in phragmoplast midline but NOT at the division site	0%, n = 0/31	77%, n = 34/44*** (p < 0.00001)	0%, n = 0/27 (ns)	0%, n = 0/40 (ns)

Table 2. POK1 and TAN1 or TAN1(28-33) localization to the division site in *tan1 air9* double mutants. Statistically significant differences were determined using Fisher's exact test. NS indicates not significant. Brown represents dual localization of YFP-POK1 and either CFP-TAN1 or CFP-

24

724 TAN1(28-33A), magenta is YFP-POK1 alone, green is CFP-TAN1(28-33A) alone, blue lines are
725 microtubules, and light gray represents the cell plate in schematics.
726

Schematic	Description	*tan1 air9* CFP-TAN1, N = 20 plants	*tan1 air9* CFP-TAN1(28-33A), N = 22 plants
	PPB, Both POK1 and TAN1	72%, n = 59/82	41%, n = 32/79 *** (p = 0.001)
	PPB, POK1 only	6%, n = 5/82	16%, n = 13/79* (p = 0.461)
	Metaphase, Both POK1 and TAN1 at the division site	100%, n = 13/13	58%, n = 11/19** (p = 0.0104)
	Early Telophase, Both POK1 and TAN1 at the division site	100%, n = 14/14	39%, n = 12/31*** (p = 0.0001)
	Early Telophase, Both POK1 and TAN1 at the division site, POK1 in the phragmoplast midline	0%, n = 0/14	26%, n = 8/31* (p = 0.0436)
	Early Telophase, NO POK1 or TAN1 at division site or phragmoplast midline	0%, n = 0/14	35%, n = 11/31** (p = 0.098)
	Late Telophase, Both POK1 and TAN1 at the division site only	95%, n = 60/63	71%, n = 42/59*** (p = 0.0004)

25

	Late Telophase, POK1 and TAN1 at the division site and POK1 in the phragmoplast midline	5%, n = 3/63	19%, n = 11/59* (p = 0.022)
	LateTelophase, TAN1 only at the division site	0%, n= 0/63	7%, n = 4/59 (NS, p = 0.0518)
	Late Telophase, Neither TAN1 or POK1 at division site or in the phragmoplast midline	0%, n = 0/63	3%, n = 2/59 (NS, p =0.2318)

727
728
729
730
731
732
733
734
735
736
737
738
739
740
741
742
743
744
745
746
747

Supplementary Figures
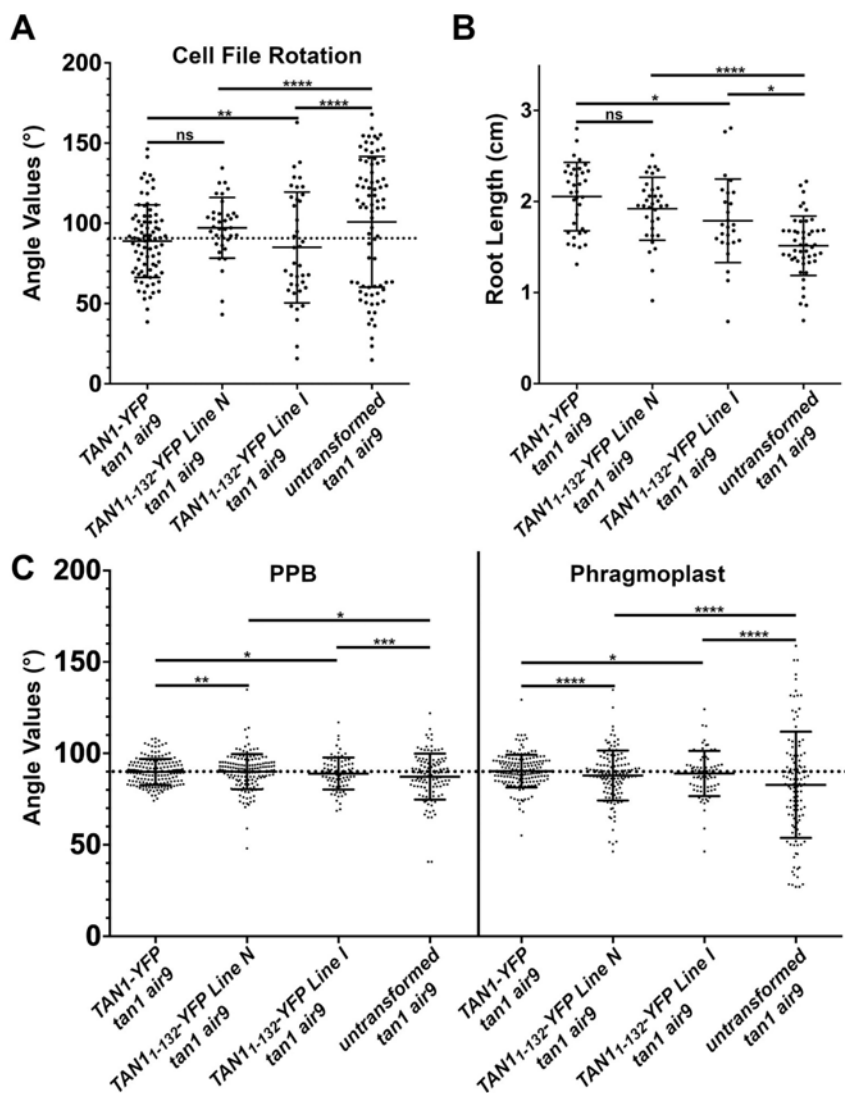
Supplementary Figure 1. *p35S:TAN1$_{1-132}$-YFP tan1 air9* lines show significant rescue compared to untransformed *tan1 air9* double mutants. A) Cell file rotation angles of *tan1 air9* double mutants expressing *p35S:TAN1-YFP* (left), two *p35S:TAN1$_{1-132}$-YFP* transgenic lines designated as line N (center left) and line I (center right) and untransformed *tan1 air9* plants (right) n > 6 plants for each genotype. Angle variances were compared with Levene's test. B) Root length measurements from 8 days after stratification of *tan1 air9* double mutants expressing p*35S:TAN1-YFP* (left), two *p35S:TAN1$_{1-132}$-YFP* transgenic lines (middle) and untransformed plants (right), n > 13 plants for each genotype, compared by two-tailed t-test with Welch's correction. C) PPB and phragmoplast angle measurements in dividing root cells of *tan1 air9* double mutants expressing p*35S:TAN1-YFP* (left), two *p35S:TAN1$_{1-132}$-YFP* transgenic lines (middle) and untransformed plants (right), n > 23 plants of each genotype. Angle variations compared with F-test. ns indicates not significant, * P-value <0.05, ** P-value <0.01, **** P-value <0.0001.
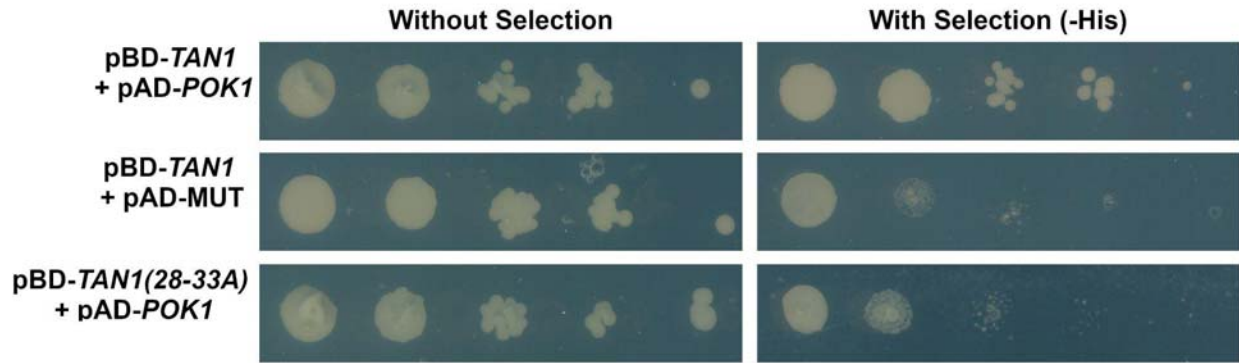
27

764
765
766

767
768
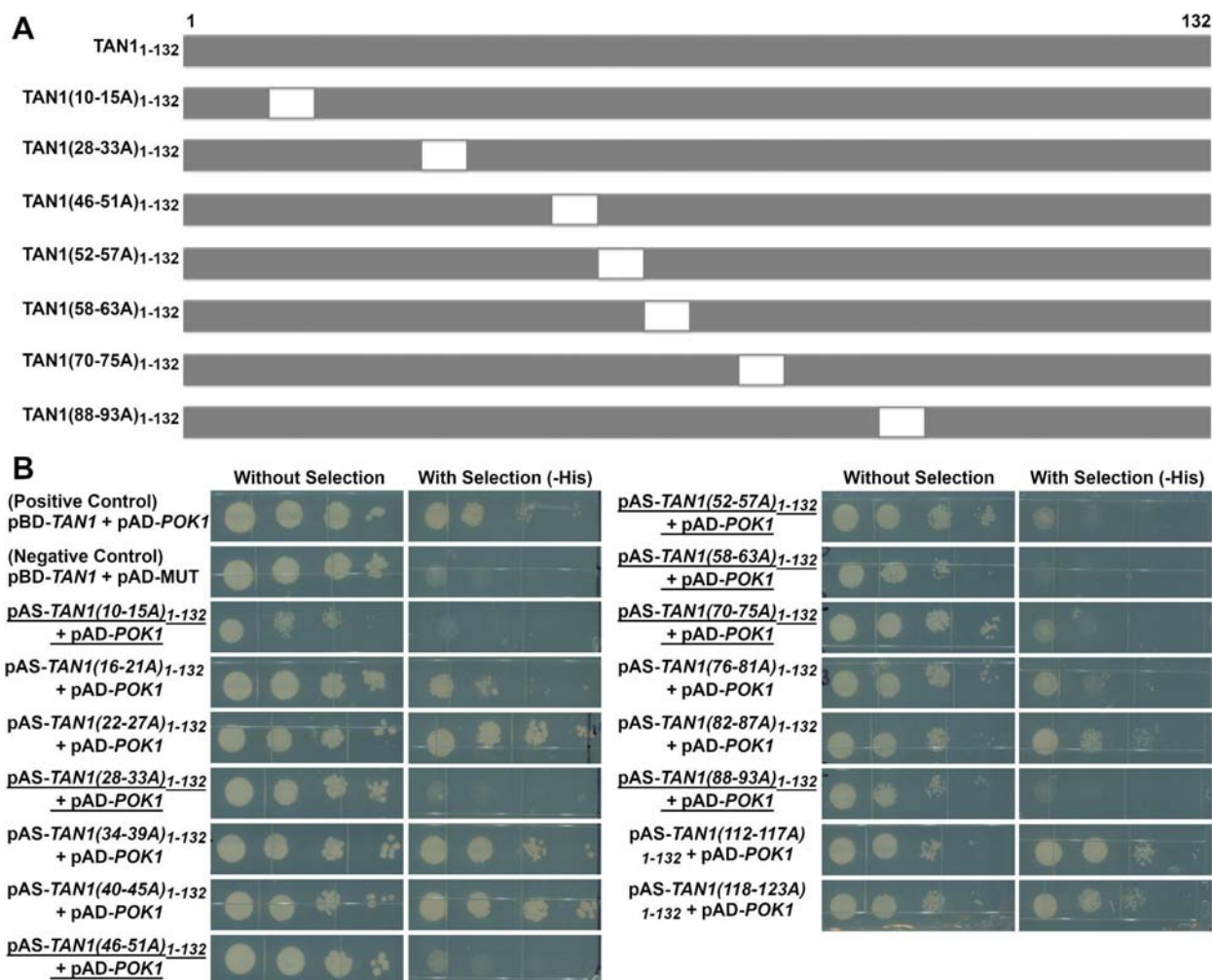
Supplementary Figure 2. Yeast-two-hybrid interactions between POK1 (C-terminal amino acids 1683-2066, as previously described (Müller et al., 2006; Rasmussen et al., 2011; Lipka et al., 2014) **) and TAN1$_{1-132}$ alanine scanning constructs.** A) Diagram of alanine scanning constructs that showed loss of interaction with POK1 by yeast-two-hybrid. The location of the six alanine substitutions within each TAN1$_{1-132}$ construct are represented by white boxes. B) Yeast-two-hybrid results of screen for loss of interaction with POK1. Underlined constructs showed loss of interaction with POK1. Alanines 64-69 and 106-111 were not completed and not included in the yeast-two-hybrid.
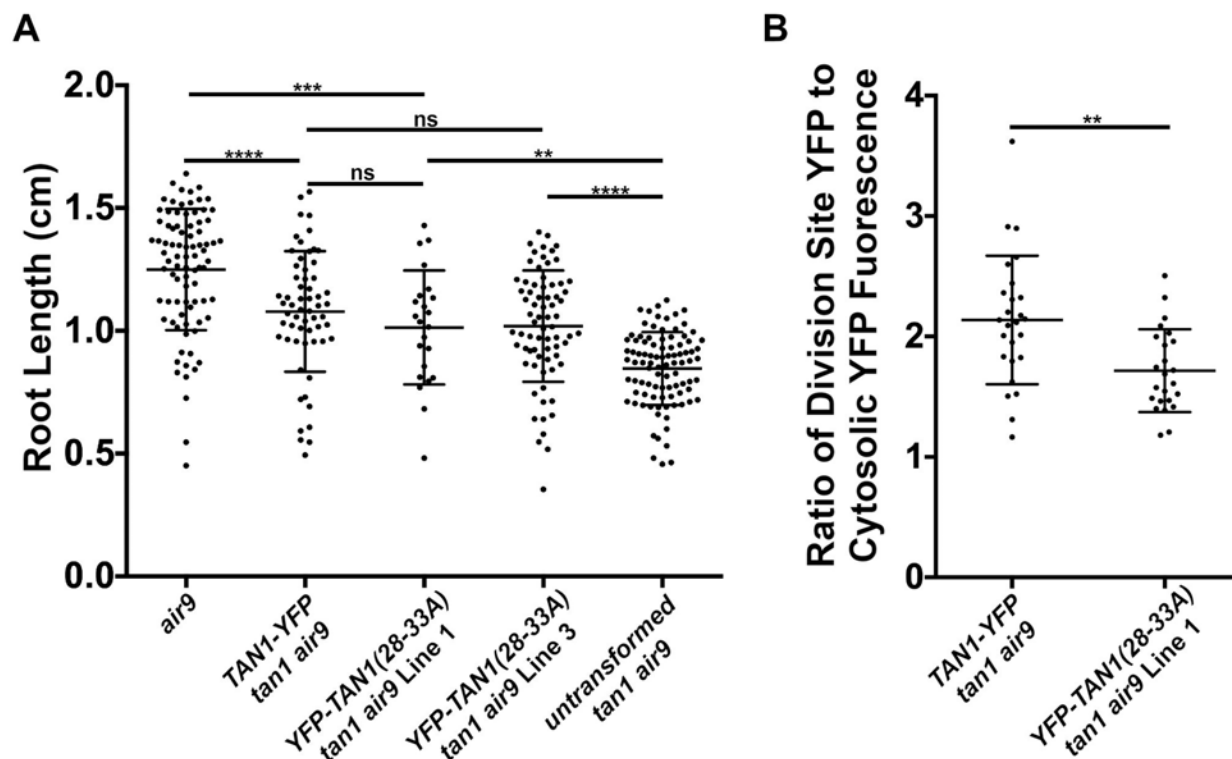
777
778
779

28

780
781
Supplementary Figure 3. Yeast-two-hybrid interactions between TAN1 and POK1 (C-terminal amino acids 1683-2066, as previously described (Müller et al., 2006; Rasmussen et al., 2011; Lipka et al., 2014) **) and TAN1(28-33A).** Full-length TAN1(28-33A) does not interact with POK1 by yeast-two-hybrid.
786

787
788

789
790

Supplementary Figure 4. *p35S:YFP-TAN1(28-33A) tan1 air9* **lines show significant rescue compared to untransformed** *tan1 air9,* **but less accumulation of YFP-TAN1(28-33A) during telophase.** A) Root length measurements from 8 days after stratification of *air9* single mutants (left), tan*1 air9* double mutants expressing *p35S:TAN1-YFP* (second from the left), two *p35S:YFP-TAN1(28-33A)-YFP* transgenic lines designated as line 1 (center) and line 3 (second from the right), and untransformed plants (right), n > 22 plants for each genotype, compared by two-tailed t-test with Welch's correction. B) Ratio of TAN1-YFP or TAN1(28-33A)-YFP fluorescence at the division site to cytosolic fluorescence from *tan1 air9* plants expressing *p35S:TAN1-YFP* (left) or *p35S:YFP-TAN1(28-33A)* (right) during telophase, n >12 plants for each genotype. Asterisks indicate a significant difference as determined by Mann-Whitney U test. ns indicates not significant, ** P-value <0.01, *** P-value <0.001, **** P-value <0.0001. Note: TAN1-YFP fluorescence measurements are the same as those used for the telophase fluorescence measurements in supplementary figure 5E.

803
804
805
806
807
808
809
810
811

30

812
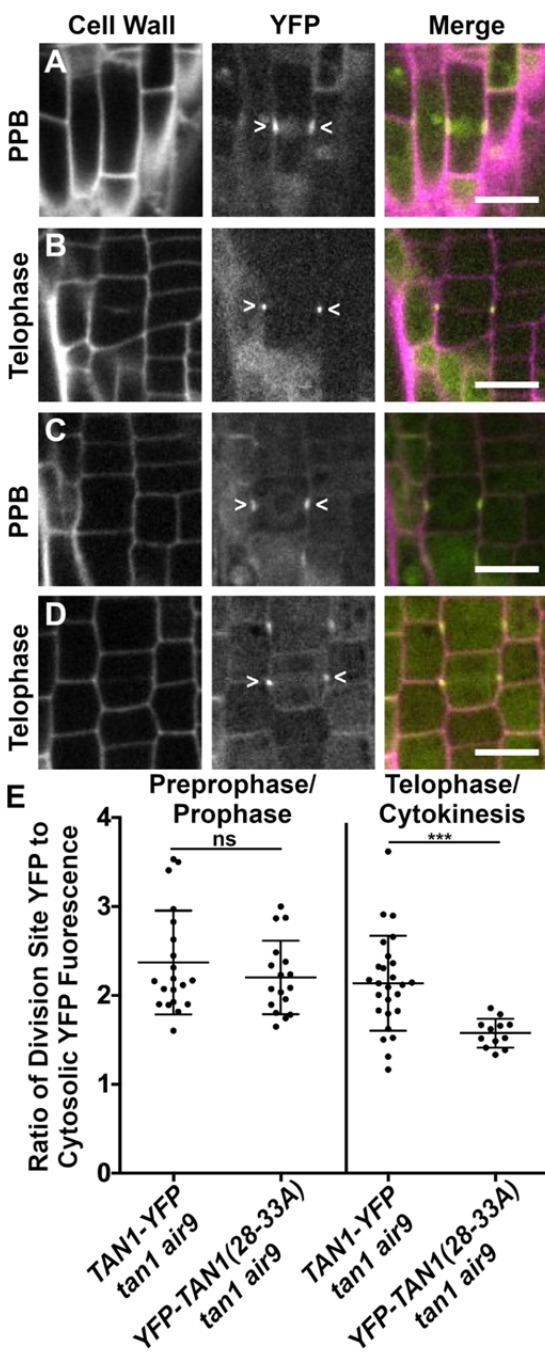
Supplementary Figure 5. YFP-TAN1(28-33A) localizes to the division site in preprophase or prophase and with reduced fluorescence during telophase in *tan1 air9* mutants. Propidium iodide stained *tan1 air9* plants expressing *p35S:TAN1-YFP* in (A) preprophase or prophase (B) telophase or cytokinesis. *tan1 air9* plants expressing *p35S:YFP-TAN1(28-33A)* in (C) preprophase or prophase (D) telophase or cytokinesis. The division site is indicated by arrowheads in the YFP panels. Bars = 10 μm. E) TAN1-YFP or TAN1(28-33A)-YFP ratio of the division site versus cytosolic fluorescence intensity from *tan1 air9* plants expressing *p35S:TAN1-YFP* or *p35S:YFP-TAN1(28-33A)* during preprophase or prophase and telophase or cytokinesis, n >5 plants for each genotype. Ratios compared with Mann-Whitney U test. ns indicates not significant, *** P-value <0.001.

847
848

849
850
851
852
853
854

31

855
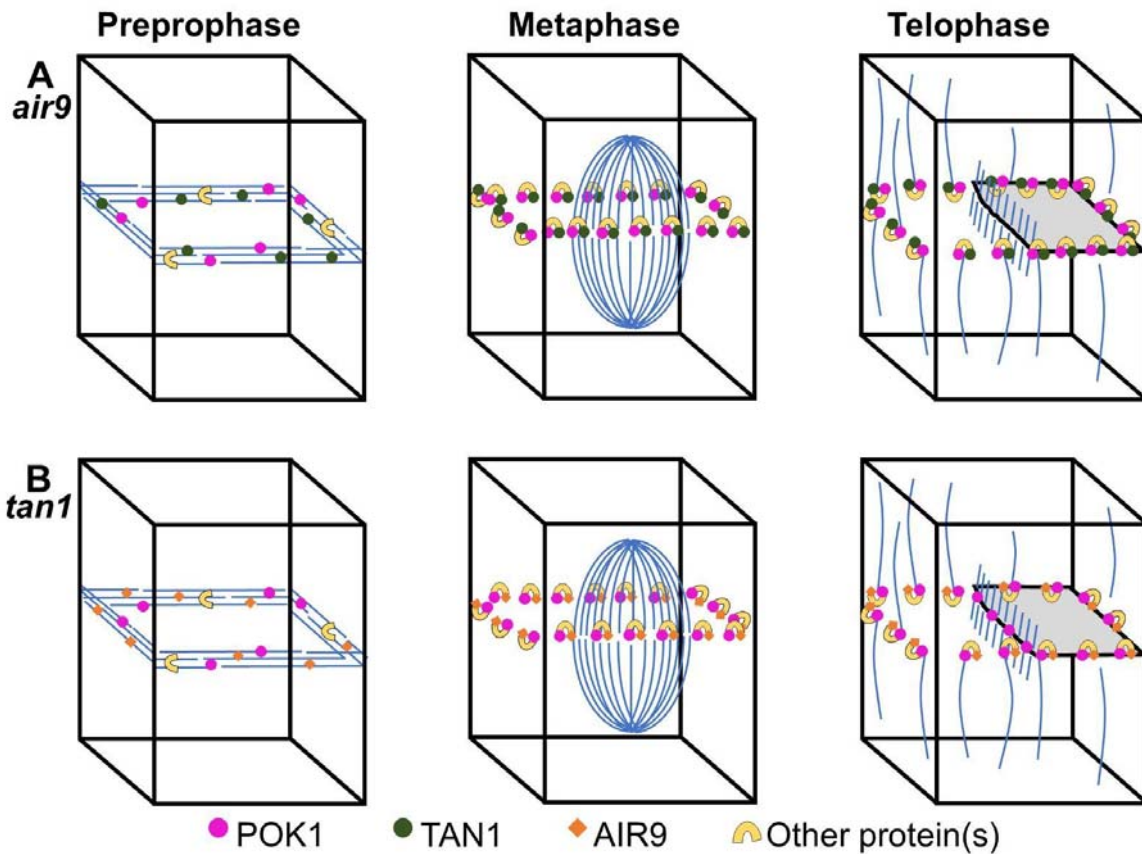
Supplementary Figure 6. A model of POK1 localization in *tan1* and *air9* single mutants. A) In *air9* single mutants TAN1 and POK1 are recruited to the PPB and their interaction with one another and other proteins stabilizes TAN1 and POK1 at the division site. B) In *tan1* single mutants AIR9 and POK1 are recruited to the PPB. POK1 is potentially stabilized at the division site either by interacting directly with AIR9 or another protein recruited to the division site by AIR9. POK1 tends to accumulate in the phragmoplast midline in *tan1* single mutants, which may reflect that POK1 is not as efficiently recruited to the division site in the absence of TAN1.

864

865

866

```
867   A. thaliana       MVARTPQKQRKVAM-----VVPPLNSDLLKETINKVDKCMERLQELQYTIAGGTKVVSGV
868   O. sativa         MVARSPDARRSRQTAAAAAAAAALNPALVRETLKKVDRCMARLQELQYTVAGGAKVVSGV
869   Z. mays           MVARSPNAKPDRQKAAALAAAAALNPALLRETLKKVDRCMARLQELQYTVAGGAKVVSGV
870   S. bicolor        MVARSPNAKPDRQTAAALAAAAALNPALVRETLKKVDRCMARLQELQYTVAGGAKVVSGV
871   S. lycopersicum   MVARTPPKLQNKKM-----VVPPLNPILLRETLNKVDKCMARLQELQYTVTGGHKVISGV
872   B. napus          MVARTPQMQRRVAM-----VVPPLNTELLKETINKVDKCMERLQELQYTIAGGTKVVSGV
873                     ****:*          ....**. *:.**::***.** ********::** **:***
```

874

Supplementary Figure 7. Alignments of amino acids 1-55 of *A. thaliana* TAN1 with TAN1 homologs from other plant species. Amino acids 28-33 of Arabidopsis TAN1 and amino acids that align with them in other plant species are highlighted in green. "*" indicates residues are fully conserved, ":" indicates strong conservation of properties across species, and "." indicates weak conservation of properties across species.

880

881

882   **Supplementary Table 1. Primers used for cloning and genotyping.**
883

Primer Name	Sequence
ATRP	ATCTCTTAGGAACCAAAACCGGACGCTGT
ATLP	GATCCGTTACGAAAGTGAACACCTTTATC
JL202	CATTTTATAATAACGCTGCGGACATCTAC
AIR9-5RP	TGGATCAGCTGCAACATTATTC
AIR9-5LP	ATTAACATTTTGCAACGCAGG
LBb1.3	ATTTTGCCGATTTCGGAAC
Ds5-4	TACGATAACGGTCGGTACGG
AtTAN 733-CDS Rw	AAATAGAGGGTTCGGAAAAAGAACC
AIR9 gnm7511 R	CCTCCAGTATATGAAGCAACAAAGC
AIR9_cDNA 2230 F	GATGAGGAATATATGTTATCTTTAGATG
Ala_Scan_FOR	GCCGTCACAGATAGATTGGCT
Ala_Scan_Rev	GAAAGCAACCTGACCTACAGG
Ala_02_FOR	GCTGCTGCCGCTGCCGCTGTGCCTCCTCTCAACTCAGAT
Ala_02_Rev	AGCGGCAGCGGCAGCAGCCTGCTTCTGTGGGGTTCT
Ala_03_FOR	GCTGCTGCCGCTGCCGCTGATCTTCTCAAGGAAACGATCAAC
Ala_03_REV	AGCGGCAGCGGCAGCAGCCACCATCGCCACTTTCCT
Ala_04_FOR	GCTGCTGCCGCTGCCGCTATCAACAAGGTTGATAAATGTATGGAA
Ala_04_REV	AGCGGCAGCGGCAGCAGCTGAGTTGAGAGGAGGCACCAC
Ala_05_FOR	GCTGCTGCCGCTGCCGCTTGTATGGAAAGACTGCAAGAGCTA
Ala_05_REV	AGCGGCAGCGGCAGCAGCCGTTTCCTTGAGAAGATCTGAGTT
Ala_06_FOR	GCTGCTGCCGCTGCCGCTGAGCTACAGTACACAATTGCAGGA
Ala_06_REV	AGCGGCAGCGGCAGCAGCTTTATCAACCTTGTTGATCGTTTCCTT
Ala_07_FOR	GCTGCTGCCGCTGCCGCTGCAGGAGGAACCAAAGTTGTC
Ala_07_REV	AGCGGCAGCGGCAGCAGCTTGCAGTCTTTCCATACATTTATCAAC
Ala_08_FOR	GCTGCTGCCGCTGCCGCTGTCTCTGGTGTGAACCTTAGC
Ala_08_REV	AGCGGCAGCGGCAGCAGCAATTGTGTACTGTAGCTCTTGCAG
Ala_09_FOR	GCTGCTGCCGCTGCCGCTAGCCCTCGAAGCACTAGA
Ala_09_REV	AGCGGCAGCGGCAGCAGCAACTTTGGTTCCTCCTGCAAT
Ala_10_FOR	GCTGCTGCCGCTGCCGCTATTTACTTGAAGACTAGTCTTAGATGCAAG
Ala_10_REV	AGCGGCAGCGGCAGCAGCAAGGTTCACACCAGAGACAAC
Ala_12_FOR	GCTGCTGCCGCTGCCGCTACTTTAAGGATCAAGAATGCTACTAATAAG
Ala_12_REV	AGCGGCAGCGGCAGCAGCACTAGTCTTCAAGTAAATTCTAGTGCT
Ala_13_FOR	GCTGCTGCCGCTGCCGCTGCTACTAATAAGAAATCTCCAGTAGGG
Ala_13_REV	AGCGGCAGCGGCAGCAGCTTCTTGCTTGCATCTAAGACTAGT
Ala_14_FOR	GCTGCTGCCGCTGCCGCTCCAGTAGGGAAGTTTCCTGCT
Ala_14_REV	AGCGGCAGCGGCAGCAGCATTCTTGATCCTTAAAGTTTCTTGCTT
Ala_15_FOR	GCTGCTGCCGCTGCCGCTGCTTCCTCACCAGGAGATTGG
Ala_15_REV	AGCGGCAGCGGCAGCAGCAGATTTCTTATTAGTAGCATTCTTGATCCT
Ala_16_FOR	GCTGCTGCCGCTGCCGCTTTGGAGGAAAATGTCACTCCCA
Ala_16_REV	AGCGGCAGCGGCAGCAGCAGGAAACTTCCCTACTGGAGA
Ala_17_FOR	GCTGCTGCCGCTGCCGCTCCAGCAATGCTACTAGGAGAG
Ala_17_REV	AGCGGCAGCGGCAGCAGCATCTCCTGGTGAGGAAGCAGG
Ala_19_FOR	GCTGCTGCCGCTGCCGCTTTTACAAGCCTCACAGGTCACA
Ala_19_REV	AGCGGCAGCGGCAGCAGCTCCTAGTAGCATTGCTGGGAG
Ala_20_FOR	GCTGCTGCCGCTGCCGCTACAAGAGACATTGTGGACGCC
Ala_20_REV	AGCGGCAGCGGCAGCAGCGATTTCATTTACAGTCTCTCCTAGTAGCAT
NpTANSacIFor	gtatgagctccggtagagttgaaccag
NpTANceruleanRev	cctcgcccttgctcaccatcttctatatatatttctttta
NpTANceruleanFor	taaagaaaatatatatagaagatggtgagcaagggcgagg
CeruleanpEarleyRev	ggcccgcggtaccgtccttgtacagctcgtccatgc
CeruleanpEarleyFor	gcatggacgagctgtacaaggacggtaccgcgggcc
pEarleyOCSPstIRev	ccatctgcagctgctgagcctcgacat
AtExon1_1For	ctcaactcagatcttctcaaggaaacg
At255AfterStopRev	gcatagtggtaccctcaaattacacc

884
885
886

34

887

888

Parsed Citations

Bellinger, M.A, Uyehara, A.N., Martinez, P., McCarthy, M.C., and Rasmussen, C.G. (2021). Cell cortex microtubules contribute to division plane positioning during telophase in maize. Cold Spring Harbor Laboratory: 2021.01.11.426230.
Google Scholar: Author Only Title Only Author and Title

Buschmann, H., Chan, J., Sanchez-Pulido, L., Andrade-Navarro, M.A, Doonan, J.H., and Lloyd, C.W. (2006). Microtubule-associated AIR9 recognizes the cortical division site at preprophase and cell-plate insertion. Curr. Biol. 16: 1938–1943.
Google Scholar: Author Only Title Only Author and Title

Buschmann, H., Dols, J., Kopischke, S., Peña, E.J., Andrade-Navarro, M.A, Heinlein, M., Szymanski, D.B., Zachgo, S., Doonan, J.H., and Lloyd, C.W. (2015). Arabidopsis KCBP interacts with AIR9 but stays in the cortical division zone throughout mitosis via its MyTH4-FERM domain. J. Cell Sci. 128: 2033–2046.
Google Scholar: Author Only Title Only Author and Title

Chugh, M., Reißner, M., Bugiel, M., Lipka, E., Herrmann, A, Roy, B., Müller, S., and Schäffer, E. (2018). Phragmoplast Orienting Kinesin 2 Is a Weak Motor Switching between Processive and Diffusive Modes. Biophys. J. 115: 375–385.
Google Scholar: Author Only Title Only Author and Title

Cleary, A.L. and Smith, L.G. (1998). The Tangled1 gene is required for spatial control of cytoskeletal arrays associated with cell division during maize leaf development. Plant Cell 10: 1875–1888.
Google Scholar: Author Only Title Only Author and Title

Clough, S.J. and Bent, A.F. (1999). Floral dip : a simplified method for Agrobacterium-mediated transformation of Arabidopsis thaliana. 16: 735–743.
Google Scholar: Author Only Title Only Author and Title

Dixit, R. and Cyr, R.J. (2002). Spatio-temporal relationship between nuclear-envelope breakdown and preprophase band disappearance in cultured tobacco cells. Protoplasma 219: 116–121.
Google Scholar: Author Only Title Only Author and Title

Earley, K.W., Haag, J.R., Pontes, O., Opper, K., Juehne, T., Song, K., and Pikaard, C.S. (2006). Gateway-compatible vectors for plant functional genomics and proteomics. Plant J. 45: 616–629.
Google Scholar: Author Only Title Only Author and Title

Facette, M.R., Rasmussen, C.G., and Van Norman, J.M. (2018). A plane choice: coordinating timing and orientation of cell division during plant development. Curr. Opin. Plant Biol. 47: 47–55.
Google Scholar: Author Only Title Only Author and Title

Fan, H.Y., Hu, Y., Tudor, M., and Ma, H. (1997). Specific interactions between the K domains of AG and AGLs, members of the MADS domain family of DNA binding proteins. Plant J. 12: 999–1010.
Google Scholar: Author Only Title Only Author and Title

Fisher, C.L. and Pei, G.K. (1997). Modification of a PCR-based site-directed mutagenesis method. Biotechniques 23: 570–1, 574.
Google Scholar: Author Only Title Only Author and Title

Herrmann, A, Livanos, P., Lipka, E., Gadeyne, A, Hauser, M.-T., Van Damme, D., and Müller, S. (2018). Dual localized kinesin-12 POK2 plays multiple roles during cell division and interacts with MAP65-3. EMBO Rep. 19: e46085.
Google Scholar: Author Only Title Only Author and Title

Hoshino, H., Yoneda, A, Kumagai, F., and Hasezawa, S. (2003). Roles of actin-depleted zone and preprophase band in determining the division site of higher-plant cells, a tobacco BY-2 cell line expressing GFP-tubulin. Protoplasma 222: 157–165.
Google Scholar: Author Only Title Only Author and Title

Hwang, J.-U., Vernoud, V., Szumlanski, A, Nielsen, E., and Yang, Z. (2008). A tip-localized RhoGAP controls cell polarity by globally inhibiting Rho GTPase at the cell apex. Curr. Biol. 18: 1907–1916.
Google Scholar: Author Only Title Only Author and Title

Karahara, I., Suda, J., Tahara, H., Yokota, E., Shimmen, T., Misaki, K., Yonemura, S., Staehelin, L.A., and Mineyuki, Y. (2009). The preprophase band is a localized center of clathrin-mediated endocytosis in late prophase cells of the onion cotyledon epidermis. Plant J. 57: 819–831.
Google Scholar: Author Only Title Only Author and Title

Kirik, V., Herrmann, U., Parupalli, C., Sedbrook, J.C., Ehrhardt, D.W., and Hülskamp, M. (2007). CLASP localizes in two discrete patterns on cortical microtubules and is required for cell morphogenesis and cell division in Arabidopsis.: 4416–4425.
Google Scholar: Author Only Title Only Author and Title

Kojo, K.H., Higaki, T., Kutsuna, N., Yoshida, Y., Yasuhara, H., and Hasezawa, S. (2013). Roles of cortical actin microfilament patterning in division plane orientation in plants. Plant Cell Physiol. 54: 1491–1503.
Google Scholar: Author Only Title Only Author and Title

Kumari, P., Dahiya, P., Livanos, P., Zergiebel, L., Kölling, M., Poeschl, Y., Stamm, G., Hermann, A, Abel, S., Müller, S., and Bürstenbinder, K. (2021). IQ67 DOMAIN proteins facilitate preprophase band formation and division-plane orientation. Nat Plants 7: 739–747.
Google Scholar: Author Only Title Only Author and Title

Lee, Y.-R.J., Hiwatashi, Y., Hotta, T., Xie, T., Doonan, J.H., and Liu, B. (2017). The Mitotic Function of Augmin Is Dependent on Its Microtubule-Associated Protein Subunit EDE1 in Arabidopsis thaliana. Curr. Biol. 27: 3891–3897.e4.
Google Scholar: Author Only Title Only Author and Title

Lee, Y.-R.J. and Liu, B. (2019). Microtubule nucleation for the assembly of acentrosomal microtubule arrays in plant cells. New Phytol. 222: 1705–1718.
Google Scholar: Author Only Title Only Author and Title

Lee, Y.-R.J., Li, Y., and Liu, B. (2007). Two Arabidopsis phragmoplast-associated kinesins play a critical role in cytokinesis during male gametogenesis. Plant Cell 19: 2595–2605.
Google Scholar: Author Only Title Only Author and Title

Lipka, E., Gadeyne, A, Stöckle, D., Zimmermann, S., De Jaeger, G., Ehrhardt, D.W., Kirik, V., Van Damme, D., and Müller, S. (2014). The Phragmoplast-Orienting Kinesin-12 Class Proteins Translate the Positional Information of the Preprophase Band to Establish the Cortical Division Zone in Arabidopsis thaliana. Plant Cell 26: 2617–2632.
Google Scholar: Author Only Title Only Author and Title

Li, S., Sun, T., and Ren, H. (2015). The functions of the cytoskeleton and associated proteins during mitosis and cytokinesis in plant cells. Front. Plant Sci. 6: 282.
Google Scholar: Author Only Title Only Author and Title

Livanos, P. and Müller, S. (2019). Division Plane Establishment and Cytokinesis. Annu. Rev. Plant Biol.
Google Scholar: Author Only Title Only Author and Title

Martinez, P., Dixit, R., Balkunde, R.S., Zhang, A, O'Leary, S.E., Brakke, K.A, and Rasmussen, C.G. (2020). TANGLED1 mediates microtubule interactions that may promote division plane positioning in maize. J. Cell Biol. 219.
Google Scholar: Author Only Title Only Author and Title

Martinez, P., Luo, A, Sylvester, A, and Rasmussen, C.G. (2017). Proper division plane orientation and mitotic progression together allow normal growth of maize. Proc. Natl. Acad. Sci. U. S. A. 114: 2759–2764.
Google Scholar: Author Only Title Only Author and Title

McMichael, C.M. and Bednarek, S.Y. (2013). Cytoskeletal and membrane dynamics during higher plant cytokinesis. New Phytol. 197: 1039–1057.
Google Scholar: Author Only Title Only Author and Title

Miki, T., Naito, H., Nishina, M., and Goshima, G. (2014). Endogenous localizome identifies 43 mitotic kinesins in a plant cell. Proc. Natl. Acad. Sci. U. S. A. 111: E1053–E1061.
Google Scholar: Author Only Title Only Author and Title

Mills, A.M. and Rasmussen, C. (2022). Action at a distance: Defects in division plane positioning in the root meristematic zone affect cell organization in the differentiation zone. bioRxiv: 2021.04.30.442137.
Google Scholar: Author Only Title Only Author and Title

Mir, R., Morris, V.H., Buschmann, H., and Rasmussen, C.G. (2018). Division Plane Orientation Defects Revealed by a Synthetic Double Mutant Phenotype. Plant Physiol. 176: 418–431.
Google Scholar: Author Only Title Only Author and Title

Müller, S., Han, S., and Smith, L.G. (2006). Two kinesins are involved in the spatial control of cytokinesis in Arabidopsis thaliana. Curr. Biol. 16: 888–894.
Google Scholar: Author Only Title Only Author and Title

Müller, S. and Jürgens, G. (2016). Plant cytokinesis-No ring, no constriction but centrifugal construction of the partitioning membrane. Semin. Cell Dev. Biol. 53: 10–18.
Google Scholar: Author Only Title Only Author and Title

Murata, T., Sano, T., Sasabe, M., Nonaka, S., Higashiyama, T., Hasezawa, S., Machida, Y., and Hasebe, M. (2013). Mechanism of microtubule array expansion in the cytokinetic phragmoplast. Nat. Commun. 4: 1967.
Google Scholar: Author Only Title Only Author and Title

Nakaoka, Y., Miki, T., Fujioka, R., Uehara, R., Tomioka, A, Obuse, C., Kubo, M., Hiwatashi, Y., and Goshima, G. (2012). An inducible RNA interference system in Physcomitrella patens reveals a dominant role of augmin in phragmoplast microtubule generation. Plant Cell 24: 1478–1493.
Google Scholar: Author Only Title Only Author and Title

van Oostende-Triplet, C., Guillet, D., Triplet, T., Pandzic, E., Wiseman, P.W., and Geitmann, A. (2017). Vesicle Dynamics during Plant Cell Cytokinesis Reveals Distinct Developmental Phases. Plant Physiol. 174: 1544–1558.
Google Scholar: Author Only Title Only Author and Title

Pan, R., Lee, Y.-R.J., and Liu, B. (2004). Localization of two homologous Arabidopsis kinesin-related proteins in the phragmoplast. Planta 220: 156–164.
Google Scholar: Author Only Title Only Author and Title

Panteris, E. (2008). Cortical actin filaments at the division site of mitotic plant cells: a reconsideration of the "actin-depleted zone." New Phytol. 179: 334–341.
Google Scholar: Author Only Title Only Author and Title

Pan, X., Fang, L., Liu, J., Senay-Aras, B., Lin, W., Zheng, S., Zhang, T., Guo, J., Manor, U., Van Norman, J., Chen, W., and Yang, Z. (2020). Auxin-induced signaling protein nanoclustering contributes to cell polarity formation. Nat. Commun. 11: 3914.
Google Scholar: Author Only Title Only Author and Title

Rasmussen, C.G. and Bellinger, M. (2018). An overview of plant division-plane orientation. New Phytol.
Google Scholar: Author Only Title Only Author and Title

Rasmussen, C.G., Sun, B., and Smith, L.G. (2011). Tangled localization at the cortical division site of plant cells occurs by several mechanisms.: 270–279.
Google Scholar: Author Only Title Only Author and Title

Russell, D.W. and Sambrook, J. (2001). Molecular cloning: a laboratory manual Third. (Cold Spring Harbor Laboratory Cold Spring Harbor, NY: Cold Spring Harbor).
Google Scholar: Author Only Title Only Author and Title

Schaefer, E., Belcram, K., Uyttewaal, M., Duroc, Y., Goussot, M., Pastuglia, M., and Bouchez, D. (2017). The preprophase band of microtubules controls the robustness of division orientation in plants. 189: 186–189.
Google Scholar: Author Only Title Only Author and Title

Smertenko, A. et al. (2017). Plant Cytokinesis: Terminology for Structures and Processes. Trends Cell Biol. 27: 885–894.
Google Scholar: Author Only Title Only Author and Title

Smertenko, A., Hewitt, S.L., Jacques, C.N., Kacprzyk, R., Liu, Y., Marcec, M.J., Moyo, L., Ogden, A., Oung, H.M., Schmidt, S., and Serrano-Romero, E.A. (2018). Phragmoplast microtubule dynamics - a game of zones. J. Cell Sci. 131: jcs203331.
Google Scholar: Author Only Title Only Author and Title

Song, H., Golovkin, M., Reddy, A.S., and Endow, S.A. (1997). In vitro motility of AtKCBP, a calmodulin-binding kinesin protein of Arabidopsis. Proc. Natl. Acad. Sci. U. S. A. 94: 322–327.
Google Scholar: Author Only Title Only Author and Title

Stöckle, D., Herrmann, A., Lipka, E., Lauster, T., Gavidia, R., Zimmermann, S., and Müller, S. (2016). Putative RopGAPs impact division plane selection and interact with kinesin-12 POK1. Nat Plants 2: 16120.
Google Scholar: Author Only Title Only Author and Title

Suetsugu, N., Yamada, N., Kagawa, T., Yonekura, H., Uyeda, T.Q.P., Kadota, A., and Wada, M. (2010). Two kinesin-like proteins mediate actin-based chloroplast movement in Arabidopsis thaliana. Proc. Natl. Acad. Sci. U. S. A. 107: 8860–8865.
Google Scholar: Author Only Title Only Author and Title

Sugimoto, K., Williamson, R.E., and Wasteneys, G.O. (2000). New Techniques Enable Comparative Analysis of Microtubule Orientation, Wall Texture, and Growth Rate in Intact Roots of Arabidopsis. Plant Physiology 124: 1493–1506.
Google Scholar: Author Only Title Only Author and Title

Van Damme, D. (2009). Division plane determination during plant somatic cytokinesis. Curr. Opin. Plant Biol. 12: 745–751.
Google Scholar: Author Only Title Only Author and Title

Vanstraelen, M., Torres Acosta, J.A., De Veylder, L., Inzé, D., and Geelen, D. (2004). A plant-specific subclass of C-terminal kinesins contains a conserved a-type cyclin-dependent kinase site implicated in folding and dimerization. Plant Physiol. 135: 1417–1429.
Google Scholar: Author Only Title Only Author and Title

Walker, K.L., Müller, S., Moss, D., Ehrhardt, D.W., and Smith, L.G. (2007). Arabidopsis TANGLED identifies the division plane throughout mitosis and cytokinesis. Curr. Biol. 17: 1827–1836.
Google Scholar: Author Only Title Only Author and Title

Wu, S.-Z., Yamada, M., Mallett, D.R., and Bezanilla, M. (2018). Cytoskeletal discoveries in the plant lineage using the moss Physcomitrella patens. Biophys. Rev.
Google Scholar: Author Only Title Only Author and Title

Xu, X.M., Zhao, Q., Rodrigo-Peiris, T., Brkljacic, J., He, C.S., Müller, S., and Meier, I. (2008). RanGAP1 is a continuous marker of

the Arabidopsis cell division plane. Proc. Natl. Acad. Sci. U. S. A. 105: 18637–18642.

Google Scholar: Author Only Title Only Author and Title